Published

This article has original data in the JCB DataViewer
http://jcb-dataviewer.rupress.org/jcb/browse/1556

JCB: Article

Action at a distance during cytokinesis

George von Dassow,[1,2] Koen J.C. Verbrugghe,[3] Ann L. Miller,[3] Jenny R. Sider,[1,5] and William M. Bement[1,3,4]

[1]Center for Cell Dynamics, Friday Harbor Laboratories, University of Washington, Seattle, WA 98250
[2]Oregon Institute of Marine Biology, University of Oregon, Eugene, OR 97420
[3]Department of Zoology and [4]Laboratory of Molecular Biology, University of Wisconsin-Madison, Madison, WI 53706
[5]Amundsen High School, Chicago, IL 60625

Animal cells decide where to build the cytokinetic apparatus by sensing the position of the mitotic spindle. Reflecting a long-standing presumption that a furrow-inducing stimulus travels from spindle to cortex via microtubules, debate continues about which microtubules, and in what geometry, are essential for accurate cytokinesis. We used live imaging in urchin and frog embryos to evaluate the relationship between microtubule organization and cytokinetic furrow position. In normal cells, the cytokinetic apparatus forms in a region of lower cortical microtubule density. Remarkably, cells depleted of astral microtubules conduct accurate, complete cytokinesis. Conversely, in anucleate cells, asters alone can support furrow induction without a spindle, but only when sufficiently separated. Ablation of a single centrosome displaces furrows away from the remaining centrosome; ablation of both centrosomes causes broad, inefficient furrowing. We conclude that the asters confer accuracy and precision to a primary furrow-inducing signal that can reach the cell surface from the spindle without transport on microtubules.

Introduction

The cytokinetic apparatus of animal cells consists of a transient, dynamic array of actin filaments and myosin-2—the contractile ring—and proteins that link it to the plasma membrane. Constriction of the contractile ring must draw the cell surface between the poles of the mitotic apparatus, separating centrosomes and sister chromosomes, to properly partition daughter cells. To ensure this, cytokinetic apparatus formation depends on spatial cues conferred upon the cortex by the mitotic apparatus.

For over a century, biologists have speculated that "astral rays" extending from the spindle poles might transmit the cytokinetic signal to the cell surface (Bütschli, 1876). With the proof that astral rays are based on microtubules (Harris, 1961), that microtubule destruction prevents cytokinesis (Beams and Evans, 1940; Hiramoto, 1956; Hamaguchi, 1975), and that opposing asters can direct cytokinesis without an intervening spindle (Rappaport, 1961), the role of astral microtubules as cytokinetic signal transmitters became ensconced in essentially all models of animal cytokinesis (for review see Burgess and Chang, 2005). A variety of specific molecular hypotheses are based on this assumption: delivery of signals from spindle to cortex via microtubule motors (Wright et al., 1993; Adams et al., 1998; Powers et al., 1998; Minestrini et al., 2003), signaling at the cortex via plus end tracking proteins (Inoue et al., 2004; Strickland et al., 2005a), and local sequestration of cytokinetic regulators at the cortex by microtubule binding (Mandato et al., 2000; Dechant and Glotzer, 2003; Birkenfeld et al., 2007).

The assumption that microtubules transmit the cytokinetic signal has also engendered long-running debates about the nature of the microtubule population responsible for signal delivery. These debates include whether astral microtubules deliver a positive or negative signal to the cortex (Wolpert, 1960; Schroeder, 1981; Rappaport, 1986), whether more microtubules contact the equatorial or the polar cortex after anaphase onset (Asnes and Schroeder, 1979; White and Borisy, 1983; Dechant and Glotzer, 2003; Motegi et al., 2006), whether more microtubule ends from opposing asters contact the equator or not (Devore et al., 1989; Harris and Gewalt, 1989; Yoshigaki, 1999), and whether dynamic properties of microtubules reaching the cortex are determinants for signal

G. von Dassow and W.M. Bement contributed equally to this paper.

Correspondence to George von Dassow: dassow@uoregon.edu

Abbreviations used in this paper: EMTB, ensconsin microtubule-binding domain; FSW, filtered seawater; mC-H2B, mCherry-histone H2B; rGBD, rhotekin GTPase-binding domain; TSA, trichostatin A.

The Rockefeller University Press $30.00
J. Cell Biol. Vol. 187 No. 6 831–845
www.jcb.org/cgi/doi/10.1083/jcb.200907090

Supplemental Material can be found at:
http://jcb.rupress.org/cgi/content/full/jcb.200907090/DC1
Original image data can be found at:
http://jcb-dataviewer.rupress.org/jcb/browse/1556

delivery (Mandato et al., 2000; Canman et al., 2003; Shannon et al., 2005; Strickland et al., 2005b; Foe and von Dassow, 2008; Odell and Foe, 2008; Vale et al., 2009). These cannot be dismissed as model system–dependent variation, as different studies in the same system have reached opposite conclusions (see Dechant and Glotzer, 2003 vs. Motegi et al., 2006 vs. Verbrugghe and White, 2007).

Newer findings change the details but not the notion that microtubules deliver the cytokinetic signal. Specifically, recent work demonstrates at least two experimentally separable cytokinetic signals: one from the spindle midzone and one from the asters (Bringmann and Hyman, 2005; Werner et al., 2007; Baruni et al., 2008; von Dassow, 2009). Also, it is now clear that activation of the small GTPase Rho at the cell equator is a conserved feature of animal cytokinesis (Bement et al., 2005), and this event is attributed to the centralspindlin complex, which consists of the kinesin MKLP1 and MgcRacGAP, working with Ect2, a Rho GEF (Yüce et al., 2005; Zhao and Fang, 2005; Kamijo et al., 2006; Nishimura and Yonemura, 2006). A popular scenario posits that MKLP transports centralspindlin along microtubules to the equatorial cortex, where it meets and activates Ect2, locally activating Rho (Saint and Somers, 2003; Somers and Saint, 2003; D'Avino et al., 2006). Delivery of a positive signal to the equator may be complemented by provision of a negative signal by dynamic microtubules that contact the cortex elsewhere (Werner et al., 2007; Chen et al., 2008; Murthy and Wadsworth, 2008; Foe and von Dassow, 2008).

Surprisingly, however, no direct proof has ever been offered that microtubules must contact the cortex for transmission of the cytokinetic signal. This is partly because it is hard to disrupt microtubules before anaphase onset without inducing metaphase arrest. Also, in large cells where signal transport might be most important, the means to clearly image microtubules extending to the cell surface have been lacking.

Here, we demonstrate the means to image and manipulate microtubules in living embryos of echinoderms and amphibians. We find that a functional cytokinetic apparatus forms and closes in the proper position in the complete absence of contact or even approach of astral microtubules with the cortex in very large, round cells. We also find that pairs of asters without an intervening spindle can specify a functional cytokinetic apparatus only when they are separated sufficiently from each other. We show that the centrosomes or asters confine the signal or its effect. Based on these and other results, we propose that distinct subsets of the mitotic apparatus collaborate to make specification of the cytokinetic apparatus both accurate and precise.

Results

Spatial organization and behavior of live microtubules during embryonic cytokinesis

To image microtubules in living urchin or *Xenopus laevis* embryos, we used three tandem GFPs fused to the ensconsin microtubule-binding domain (EMTB-3G; Faire et al., 1999). This probe, unlike fluorophore-conjugated or GFP-tubulin, enabled high-contrast, high-resolution microtubule visualization throughout the cell cycle, from the eight-cell stage on in purple urchin or sand dollar embryos (Fig. 1 and Video 1) and *X. laevis* blastomeres (Fig. S1 D and Video 2), which revealed apparently single microtubules extending to the cortex, even in large cells. Rapid microtubule growth and shrinkage were clearly evident (Fig. 1 C′ and Fig. S1 E), with microtubule growth at 16.7 ± 11 μm/min ($n = 50$) and shrinkage at 9.9 ± 2.6 μm/min ($n = 50$) in *X. laevis* embryos, which is consistent with studies of cell free extracts (e.g., Belmont et al., 1990).

Immunostaining embryos expressing EMTB-3G showed that GFP overlapped nearly completely with tubulin (Fig. S2), the sole exception being the ends of spindle midzone microtubules and the center of the midbody, which were underlabeled by EMTB-3G. The only drawback to EMTB-3G was that rapid expression in the earliest embryos caused cell cycle arrest (Fig. S1 A) or defective mitosis. However, injection of 0.05–0.1 ng/nl EMTB-3G mRNA routinely produced embryos with robust microtubule labeling and normal cell cycle progression; such embryos cleaved with no sign of mitotic errors to late blastula, whereupon they began to swim, gastrulated normally, and became morphologically normal feeding pluteus larvae (Fig. S1, B and C).

We assessed microtubule dynamics in surface and axial views of sand dollar and purple urchin embryos (Fig. 1 and Fig. 2, A–C) and in surface views of *X. laevis* embryos (Fig. 2 D, Video 2, and Fig. S1 D). In all three species, regardless of imaging plane, three observations were remarkably consistent. First, microtubules arrived in every part of the cortex, including the equator, before furrowing (Fig. 1 A, B [ii–iv], and C; Fig. 2, A′–C; and Fig. S1 D′). Second, after anaphase onset, most astral microtubules at the cortex were stable, regardless of orientation (Fig. 2, A′–C; and Fig. S1 D′). Third, astral microtubules reached the cortex in greater density outside the furrow region (Figs. 1 C, 2, and S1 D). The last point was confirmed by imaging both microtubules (with 3C-EMTB) and active Rho, the earliest known marker for cytokinetic apparatus specification (with GFP–rhotekin GTPase-binding domain [rGBD]; Benink and Bement, 2005) in *X. laevis* embryos (Fig. 2 D), which showed that microtubules arrived at the cortex before Rho activation even in very large cells, and that the Rho zone occupied a microtubule-poor region of the cortex.

Nocodazole-insensitive microtubules in living cells

Immunofluorescence analysis of fixed echinoderm zygotes (Foe and von Dassow, 2008) revealed a nocodazole-insensitive population of astral microtubules that arises at anaphase onset and that has a clear equatorial bias before furrowing. However, EMTB-3G detects apparently stable microtubules throughout the cortex in later embryos (eight-cell and beyond). We tested whether these are nocodazole insensitive by perfusing eight-cell and older EMTB-3G–expressing embryos with nocodazole. Consistent with previous results, 10–20-μM nocodazole treatment during anaphase prompted rapid loss of most astral microtubules but left a substantial fraction extending from each spindle pole (Fig. 3 and Video 3). However, in contrast to the results obtained with

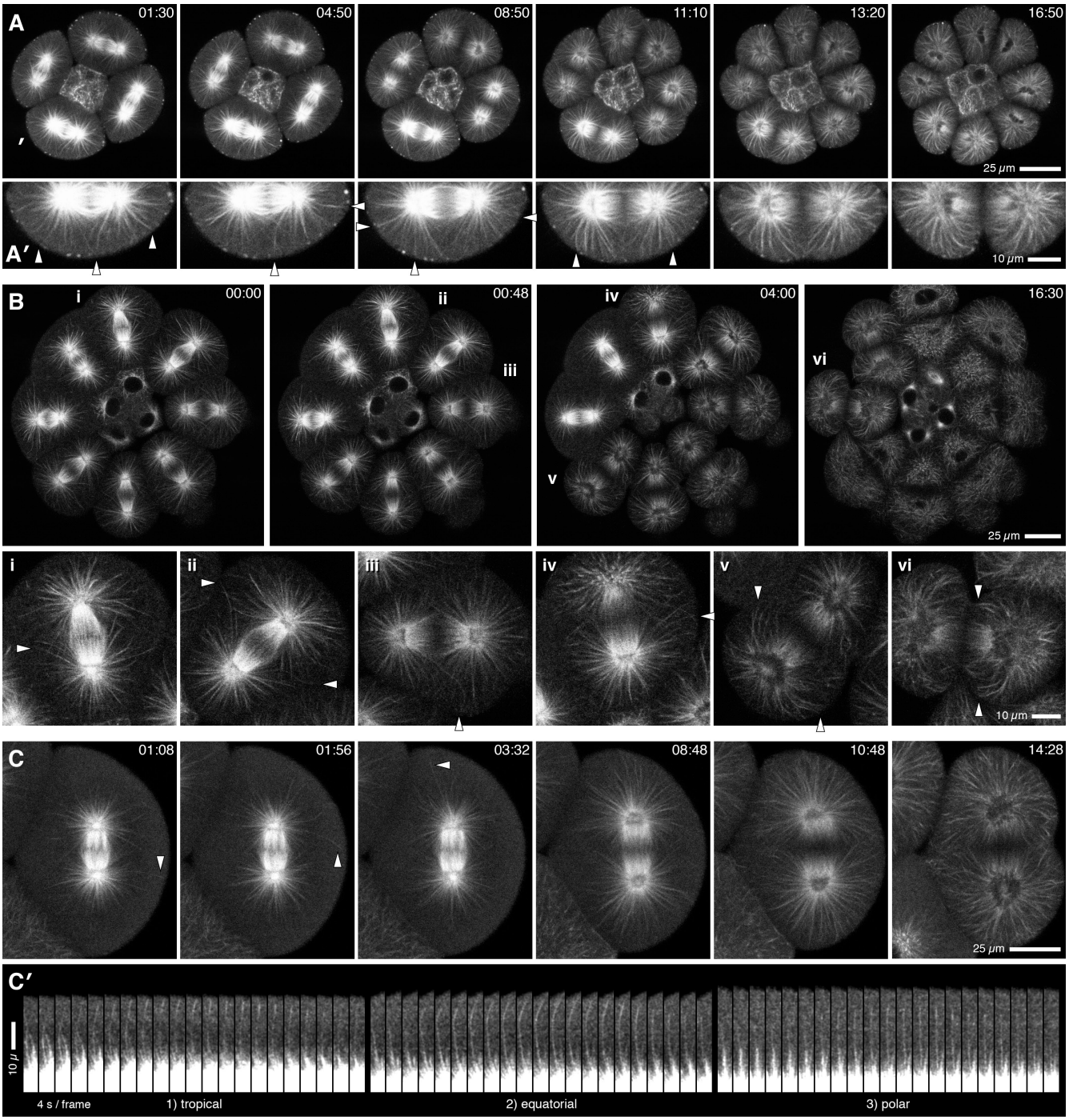

Figure 1. **Microtubules in live urchin embryos.** All panels show single confocal sections. (A and A′) 16-cell purple urchin embryo; A′ shows a 2× enlarged view of the lower cell (indicated by white mark in A). Microtubules approach the cortex everywhere before anaphase onset (1 min, 30 s); during anaphase, just before furrowing, many astral microtubules penetrate both polar and equatorial cortex (arrowheads in A′). (B) Vegetal view, 28-cell sand dollar embryo; i–vi are 2× enlarged views as indicated. Astral microtubules frequently cross spindle midplane before and during anaphase (i–iii), approach within 1 μm of the equatorial surface before furrowing (ii–iv), and curve inward as the furrow ingresses (v and vi). Arrowheads point to exemplars. (C) Eight-cell sand dollar embryo; single microtubules grow as far as the cell surface in all directions (equatorially in the 01:56 frame, tropically in the 01:08 frame, and toward the pole in the 03:32 frame). Astral microtubules reach the polar cortex most densely in anaphase (08:48) but also reach the equator before furrowing (frame 10:48). (C′) Enlargement of successive frames for microtubules indicated by arrowheads in C (intensities squared to enhance contrast). Video 1 corresponds to A–C. Time is indicated in minutes:seconds.

zygotes, in these smaller cells, there was no obvious directional bias of nocodazole-insensitive microtubules toward the equator before furrowing (Fig. 3), which indicates that these stable microtubules cannot solely explain cytokinetic pattern formation.

In the course of these experiments, we noticed that nocodazole treatment failed to prevent cytokinesis even when it prevented microtubules from approaching the cortex, either from the spindle midzone or the asters (Fig. 3 and Video 3). Every

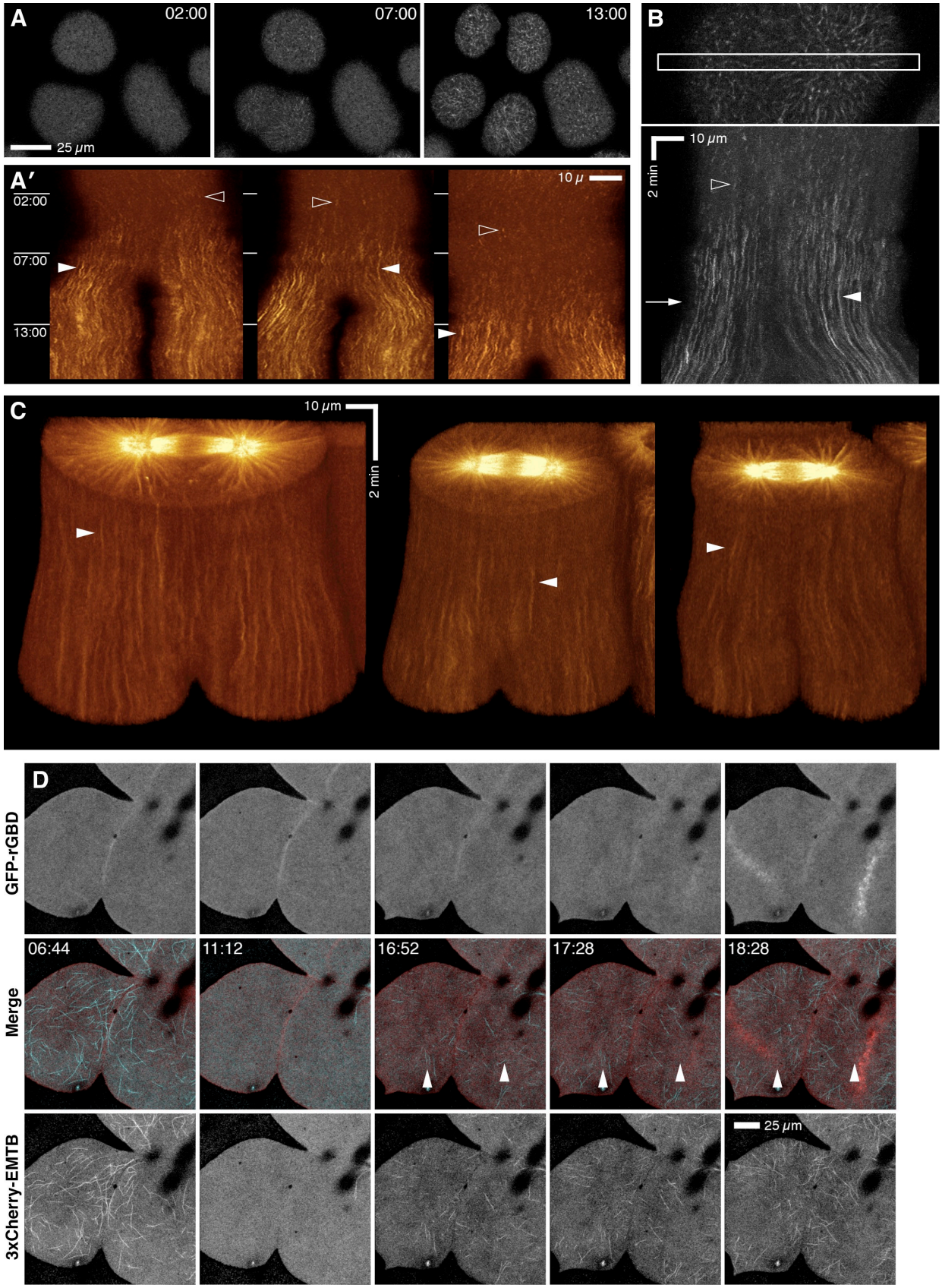

Figure 2. **The furrow forms in a microtubule-poor region.** (A) Single superficial confocal sections of a 16-cell sand dollar embryo, slightly compressed (EMTB-3G). (02:00) All three cells in metaphase; few microtubule ends are visible. (07:00) Left cell begins cleavage, right cell is still in metaphase, and the top cell has likely entered anaphase. (13:00) Right cell begins to cleave; fewer microtubules approach the cell surface (bright dots) in the incipient furrow than outside it. (A′) "Kymocubes" made by 3D rendering sequence in A; white lines denote frames in A. The whole of each of three cells is shown

cell that entered anaphase (as deduced from emergence of a dark gap between spindle halves), regardless of the extent of the surviving aster, established a well-placed furrow. This is epitomized by Fig. 3 B: cytokinesis occurred in one cell that entered anaphase just when nocodazole was added (and completely lacked long astral microtubules) but not in three metaphase-arrested cells.

Microtubule-independent delivery of the cytokinetic signal

The nocodazole results imply that cytokinetic signals can reach the cortex without the help of microtubules extending from the spindle to the cortex. But because nocodazole must be applied after anaphase onset to avoid metaphase arrest, it might be that signaling occurred in the narrow window before nocodazole took effect. Also, although nocodazole greatly shortened microtubules extending from the spindle to the cell surface, perhaps stable microtubules were still close enough to mediate equatorial delivery. To inhibit astral microtubule growth without cell cycle arrest, we therefore treated embryos with trichostatin A (TSA), an inhibitor of HDAC6 (a tubulin deacetylase) that selectively disrupts dynamic microtubules in mammalian cells (Matsuyama et al., 2002). Perfusion of urchin embryos with TSA in prophase or metaphase caused rapid collapse of the aster and usually a delay, but not an arrest, in metaphase (Fig. 4; Videos 4 and 5; and Figs. S3 and S4).

In metaphase, TSA caused the entire aster to collapse within minutes (Figs. 4, S3 B, and S4 A); as with nocodazole, anaphase cells retained a subset of stable astral microtubules (Fig. S3 B). The spindle itself often became much shorter in TSA-treated cells, and sometimes became deranged during a prolonged metaphase (e.g., Fig. S4 B). Even so, most TSA-treated cells underwent anaphase, as revealed by a widening gap in the midzone and emergence of nuclear vesicles near spindle poles (Fig. 4, A and C), or by coexpressing EMTB-3G and mCherry-histone H2B (mC-H2B; Figs. 4 B and S3 B). Although short microtubules often regrew from centrosomes in anaphase, and isolated microtubules formed in the cytoplasm (e.g., Fig. 4 C), extension of microtubules from either the spindle midzone or the poles to the cortex was not detected.

Astonishingly, the vast majority of TSA-treated cells completed cytokinesis, despite the near-total absence of astral microtubules (Fig. 4, Videos 4 and 5, and Figs. S3 B and S4). Moreover, cytokinesis occurred with unexpected fidelity; the furrow formed and closed equatorially between the modestly separated chromosomes even when the closest detectable approach by a spindle microtubule to the cell surface was >10 μm (Fig. 4 C and Fig. S4 B). Only failure to enter anaphase prevented furrowing. In a minority of cells, the ingressing furrow initially failed to separate the chromosome sets. However, in many of these, the cell corrected this error as the constricting furrow approached the spindle, either by the spindle being moved back and forth until it matched the furrow position, or by shifting the furrow toward the spindle midzone (not depicted).

These results, which were obtained by imaging a single medial optical plane, were confirmed by complete z series or surface views of live TSA-treated cells (not depicted). To complement live imaging, we treated embryos with TSA, then fixed and stained for tubulin and serine-19 phosphorylated myosin light chain (phospho-myosin; a marker for active myosin-2 and the cytokinetic apparatus). 3D reconstructions of these embryos showed clearly that a functional cytokinetic apparatus, replete with active myosin-2, forms at the equator of TSA-treated cells in the complete absence of approach of spindle microtubules to the cortex (Fig. 5), which eliminates the possibility that the apparent lack of astral microtubules seen by live cell imaging reflects either deficiencies in the EMTB-3G probe or the imaging regimen. Finally, the possibility that the cytokinetic pattern formed long before TSA took effect was ruled out by cases in which TSA was applied before metaphase; the cell depicted in Fig. S4 B, for example, never achieved long astral microtubules in this cell cycle. We find it impossible to escape the conclusion that abolishing contact between astral microtubules and the cell cortex simply does not prevent the cell from assembling a normally positioned, functional cytokinetic apparatus.

Astral microtubules focus the cytokinetic pattern

Although TSA-treated cells established accurate cytokinetic furrows, those furrows were abnormally broad, as was the distribution of active myosin-2 (e.g., Fig. S4 B and Fig. 5). We therefore assessed cytokinetic pattern formation using GFP-rGBD, alone or in combination with 3C-EMTB. The Rho zone was harder to detect in TSA-treated cells, but was definitely present (Fig. 6, C and D), which confirmed that cells can confine Rho activation to the equator without help from asters. TSA-treated cells, like normal cells, exhibited ubiquitous low-level cortical Rho activity that declined after anaphase onset (Fig. 6 D). However, the Rho zone was much wider than normal in TSA-treated cells (Fig. 6 A). Measurement

in the kymocube. Bright dots (open arrowheads in A–C) indicate brief cortical visits by microtubule ends; these predominate in metaphase. Vertical streaks (closed arrowheads in A–C) indicate kinematically stable microtubule ends, which appear before furrowing, and are scarce in the equatorial zone. (B) Kymograph of 5-μm medial strip (indicated by box) ~1 μm beneath the surface of a slightly flattened eight-cell sand dollar embryo. The arrow indicates furrow initiation time; vertical streaks above this point indicate stable microtubules at the cortex before furrowing. These are notably fewer in the equator. (C) Surface rendering of single medial sections of uncompressed sand dollar blastomeres, each covering anaphase through cytokinesis. Long streaks (stable microtubules at the cell surface) are evident well before furrowing. Broad smears appear during furrowing, notably in the area around the crotch; these reflect microtubules growing along the cortex (see also A′ and B). (D) Single superficial sections from a 6.5-h *X. laevis* embryo mosaically expressing GFP-rGBD (red) and 3C-EMTB (cyan). Surface microtubules disappear in metaphase, then reappear (16:52) ~90 s before active Rho appears in the equator (18:28). Microtubules are largely absent from a >20-μm-wide band inhabited by the Rho zone; arrows indicate equatorial microtubules that disappear during furrowing. Time is indicated in minutes:seconds.

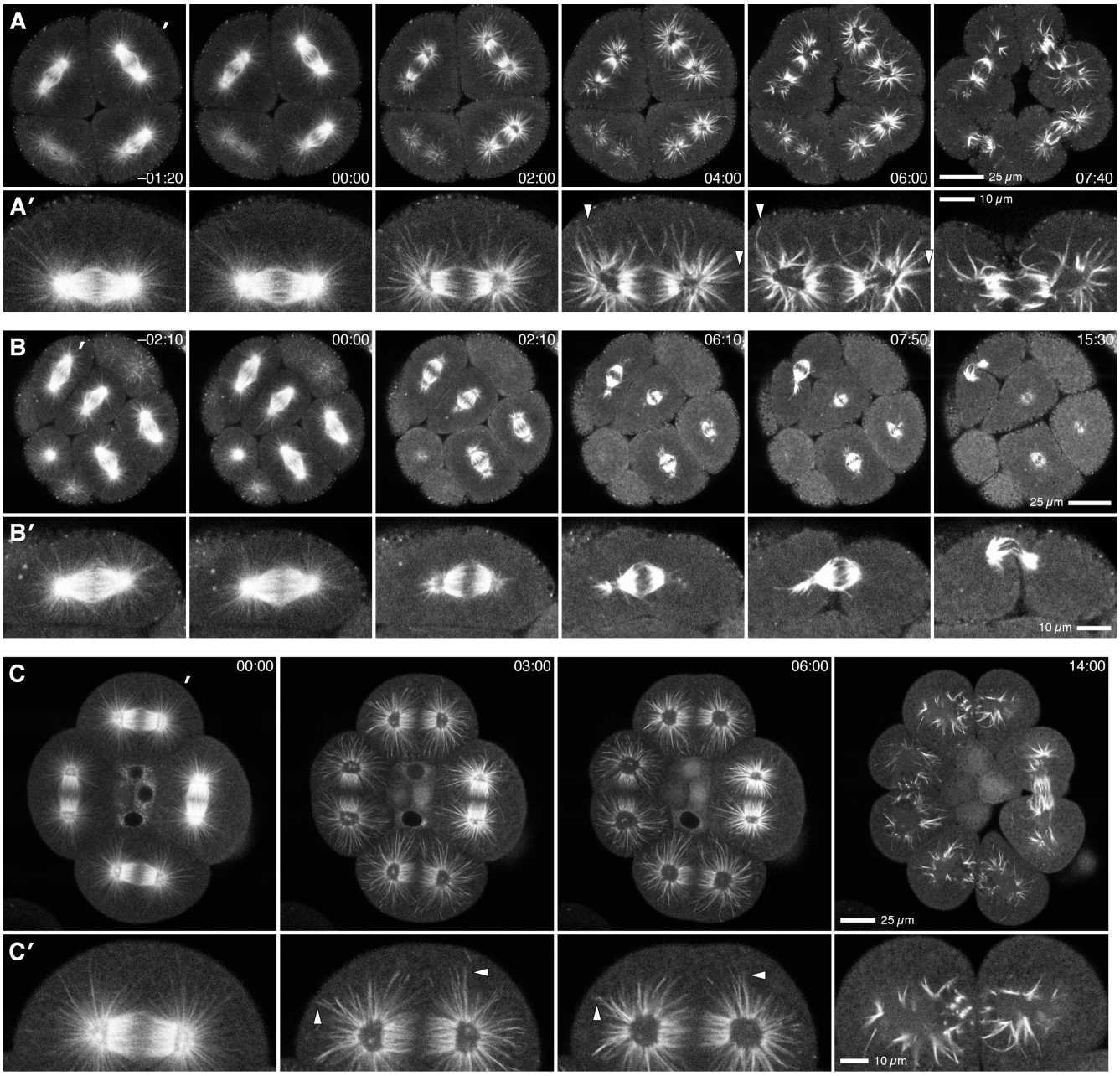

Figure 3. **Nocodazole-insensitive microtubules exhibit no orientation bias in urchin blastomeres.** (A–C) Single sections, all expressing EMTB-3G; (A′–C′) 2× enlarged views of cells indicated by the white marks in A–C. (A) Eight-cell purple urchin embryo; 20 μM nocodazole was added at time 00:00. Within 2 min, most astral microtubules disassembled; remaining microtubules are randomly oriented and most end well short of the cortex. Even so, furrowing is accurate and timely. Arrowheads indicate surviving nonequatorial astral microtubules. (B) 16-cell purple urchin embryo; 10 μM nocodazole was added at time 00:00. The top left cell entered anaphase around time 0; none of the other cells in view left metaphase nor furrowed. This one cell cleaved despite nearly complete absence of astral microtubules, and the furrow crossed the spindle midzone. (C) 16-cell sand dollar embryo; 10 μM nocodazole was added at time 00:00, at which time three of four macromeres have entered anaphase; the east cell enters anaphase shortly thereafter (03:00). In all cells, numerous astral microtubules, pointing in all directions, persist >5 min after nocodazole addition (arrowheads). Stable microtubules may approach the cortex in west and south cells (03:00), but none can be seen to do so in north and east cells; all commence furrowing at a normal time and complete cytokinesis. Note that in all cases, stable microtubules become brighter because EMTB-3G liberated by disassembly becomes available for binding. Video 3 includes A–C. Time is indicated in minutes:seconds.

of Rho zone width by curve fitting (see Materials and methods) showed that Rho activity in TSA-treated cells covered a latitude range along the cell surface on average twice as wide as in controls from the same batch of eggs (Fig. 6 B; 0.28 ± 0.14 of the pole-to-pole cell diameter in TSA-treated cells [$n = 23$] vs. 0.14 ± 0.06 in controls [$n = 29$]; $P < 0.0002$). Notably, the intensity above background integrated across the entire Rho zone was not significantly less than normal in TSA-treated cells; thus, Rho activity is diluted, not diminished, by the absence of asters.

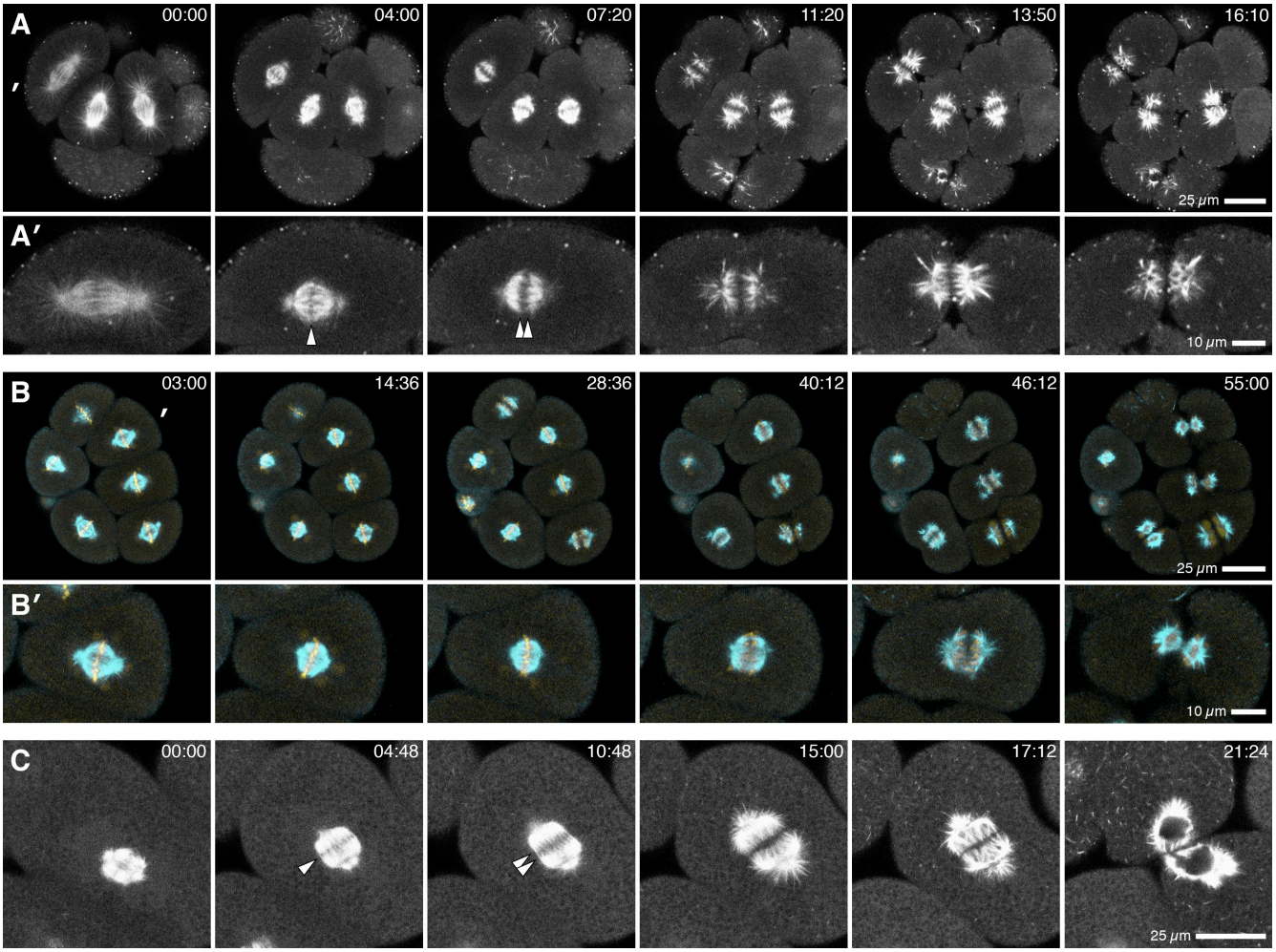

Figure 4. **Cleavage occurs despite diminution of the aster and cortical microtubules by TSA.** All panels are single confocal sections. (A) 16-cell purple urchin embryo (EMTB-3G), treated with 20 μM TSA at time 00:00. A′ shows a 2× enlarged view of the indicated cell (white mark in A). Within minutes of TSA addition in metaphase, asters were reduced to nearly nothing (04:00). Despite reduction in spindle length, cells enter anaphase (07:20) and complete cytokinesis (11:20–16:10). No microtubules connecting the mitotic apparatus to the cortex are visible (see Video 4). (B) 16-cell purple urchin embryo (cyan, EMTB-3G; yellow, mC-H2B); 15 μM TSA was added at time 00:00. After a delay in metaphase, five of six cells in focus initiate cytokinesis. B′ shows a 2× enlarged view of the indicated cell (white mark in B). (C) One cell within a 16-cell sand dollar embryo (EMTB-3G), treated with 25 μM TSA ∼10 min before time 00:00. Although the aster regrows slightly, the cortex is ∼20 μm away from the nearest spindle microtubule ends; nevertheless, cytokinesis completes accurately (see Video 4). Arrowheads in A and C indicate metaphase plate before (04:00 and 04:48), and the gap after (07:20 and 10:48), anaphase onset. Time is indicated in minutes:seconds.

Asters alone can only induce a furrow if they are far enough apart

The results of TSA treatment show that cells can accurately position the cytokinetic apparatus without the astral microtubule array. Yet numerous classical results identified the juxtaposition of two asters as the sufficient condition for furrow induction (e.g., Rappaport 1961). To resolve this contradiction, we created EMTB-3G–expressing cell fragments that contain centrosomes but lack nuclei (see Materials and methods). These anucleate cytoplasts conduct a normal centrosome cycle: duplication and separation, and cyclic alternation between a compact, dense, and dynamic aster (metaphase) and a loose aster of long, stable microtubules (interphase). Anucleate cytoplasts with two or more centrosomes exhibited a full spectrum of cytokinetic behaviors: some showed no sign of cleavage; some cleaved completely; and in some, furrows ingressed some distance before regressing (Fig. 7, A–C; and Video 6). In all cases, regardless of cytokinetic behavior, astral microtubules penetrated the cortex everywhere (as in normal cells) during anaphase and telophase, and in no case did we detect anything like a spindle between two centrosomes in an anucleate cytoplast.

The observed behavioral spectrum might suggest that asters alone can induce a furrow but that induction isn't robust under these conditions. However, we noticed that anucleate cytoplasts that manifest deeply ingressing furrows have a greater separation between adjacent asters (Fig. 7, A vs. B). This is apparent even within a single case: in Fig. 7 C, deeply ingressing furrows develop between well-separated asters, and only shallow furrows develop between closer pairs. This correlation was quantified by comparing the distance between centrosomes versus the distance from the surface, versus the extent of furrowing (see Materials and methods). As shown in Fig. 7 E, if the distance between centrosomes exceeded

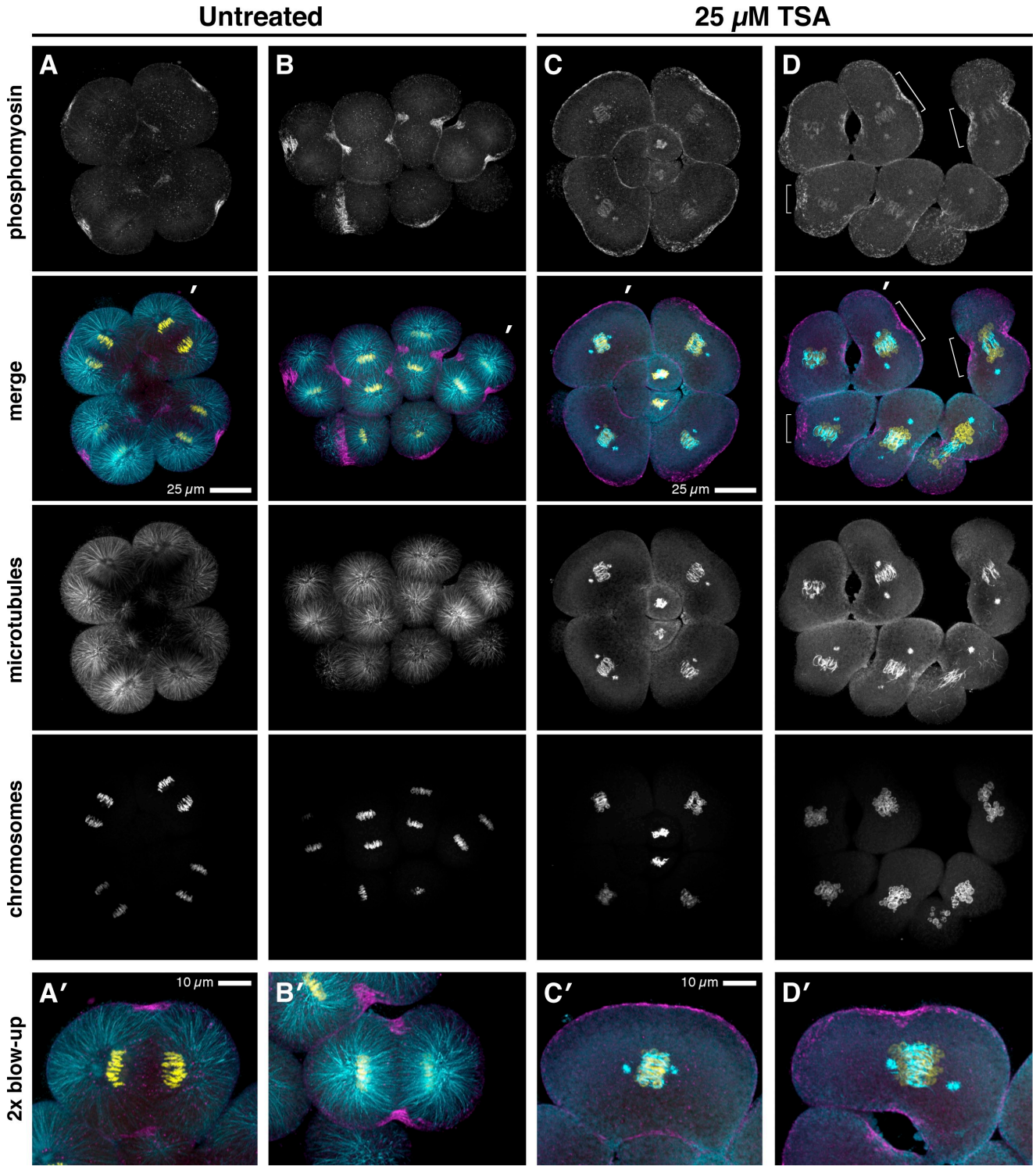

Figure 5. **Myosin occupies a wider-than-normal zone in asterless cells.** Cyan, anti-tubulin; yellow, Hoechst; magenta, anti-phospho-myosin. (A and B) Untreated 16-cell sand dollar embryos. Projection of 24 0.5-μm sections, vegetal view (A); and 19 0.6-μm sections, side view (B). (C and D) 16-cell sand dollar embryos fixed 10 min after adding 25 μM TSA. (C) A projection of 18 0.5-μm sections through the middle portion of the macromeres. (D) A projection of 28 0.5-μm sections through the middle portion of the mesomeres. A–D are from the same batch fixed at the same time. Normally, phospho-myosin is virtually absent outside of ∼10 μm furrow zone. In TSA-treated cells, phosphomyosin is not as thoroughly excluded from the poles but is still enriched equatorially, with definite zones around ingressing furrows (brackets in D), even though no spindle microtubules approach the cortex. A′–D′ are 2× enlarged views of the cells indicated by the white marks in A–D.

the distance to the cell surface, furrows ingressed deeply. If the two distances were roughly equal, only shallow furrows developed. If centrosomes were substantially closer than the distance to the surface, no furrow developed. These differences were highly significant (in both comparisons, $P < 0.001$).

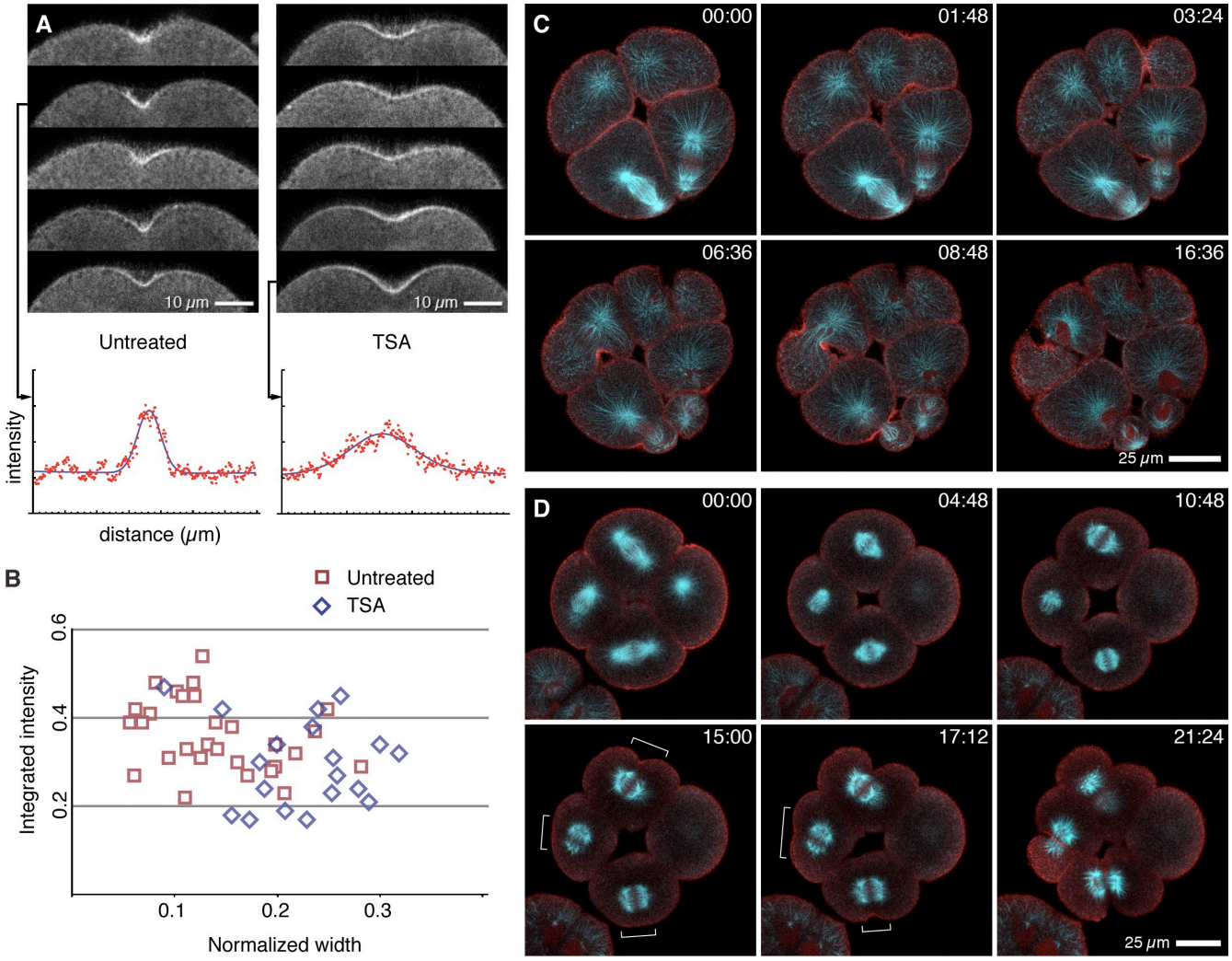

Figure 6. **Active Rho occupies a wider-than-normal zone in asterless cells.** (A) GFP-rGBD at similar stages of furrowing in control (left) and TSA-treated (right) purple urchin embryos; single confocal sections. Rho zones are broader and fainter in TSA-treated cells compared with untreated siblings, but zones are centered equatorially and match furrows. Plots show representative fits between intensity data (red) and a fit curve (blue) that measures zone width along the cell outline (see Materials and methods). (B) Measured zone widths normalized by pole-to-pole cell length, plotted against integrated intensity, minus baseline, within the curve fit as shown in A, expressed as a fraction of baseline. (C) Normal Rho zones, eight-cell purple urchin embryo (red, GFP-rGBD; cyan, 3C-EMTB). (D) Eight-cell purple urchin embryo (same probes as C) treated with 20 μM TSA at time 00:00. Uniform cortical Rho activity during metaphase (00:00) disappears as cells enter anaphase, as in normal cells (Bement et al., 2005). Rho zones (brackets) are barely detectable above background, yet furrows develop and complete with minor delay (compare times in C), which implies that cells normally express more equatorial Rho activity than they require. Time is indicated in minutes:seconds.

Asters spatially confine the cytokinetic signal

The behavior of anucleate cytoplasts confirms that asters, or the centrosomes they grow from, somehow provide enough positional information to direct furrowing. Meanwhile, nocodazole and TSA treatment show that the astral microtubules need not reach the cortex for the cell to accurately identify the appropriate furrow site, although the cytokinetic apparatus is more broadly specified in the absence of asters. These results could be reconciled if the central spindle localizes a positive signal, and the astral microtubules or centrosomes suppress cortical contractility outside the equator, thereby sharpening this signal at the cortex. A second hypothesis is that a positive signal from the spindle midzone is spatially confined by the asters or centrosomes, perhaps by interacting with astral microtubules or because something associated with centrosomes depletes or inactivates the signal in the cell interior. If the first hypothesis were correct, one would predict destruction of a single aster to broaden and strengthen the signal; if the second were correct, relatively little change in signal level is expected. Both hypotheses predict that destroying a single aster should shift the signal away from the midzone, toward the ablated aster. A third hypothesis is that asters or centrosomes generate positive signals that are summed at the equator, with or without synergistic signals from the midzone; in this case, destruction of a single aster should shift the signal away from the ablated aster, and the signal should be weakened.

We tested these predictions by destroying centrosomes in sand dollar blastomeres using a UV laser (see Materials and methods). Most singly ablated cells clearly underwent

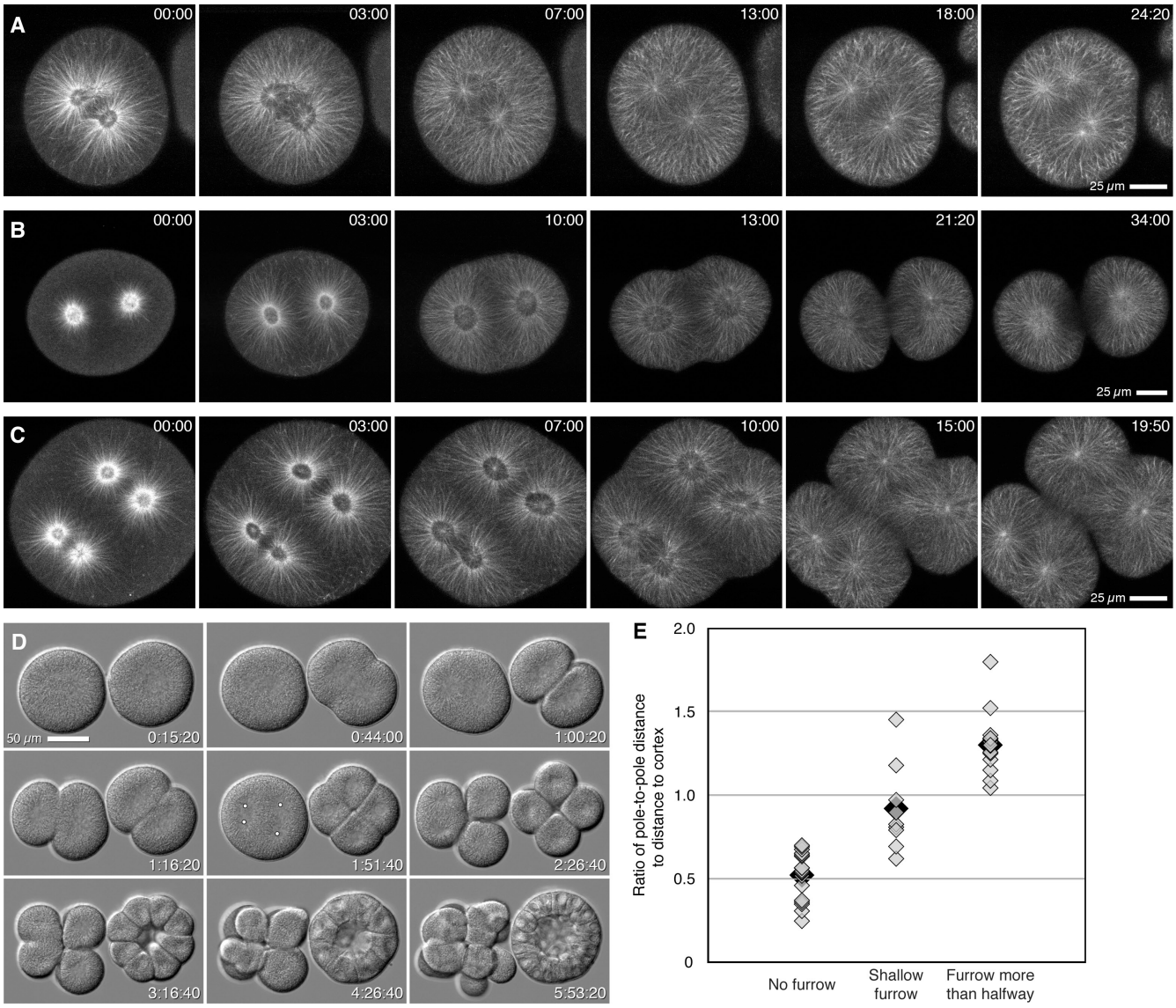

Figure 7. **Asters alone induce furrows only if they are far enough apart.** (A–C) Single-plane sequences of anucleate, centrosome-containing cytoplasts (sand dollars). (A) Anucleate cytoplast with four centrosomes, two in focus. In normal cells this size, furrowing would begin between 03:00 and 07:00, but no furrow occurs even 20 min later. Centrosomes are closer than the distance to the equator. (B) Anucleate cytoplast with two centrosomes, farther apart than the distance to the equator. A furrow initiates at the expected time and place, and proceeds to completion. (C) An anucleate cytoplast with four centrosomes variously spaced. A deeply ingressing furrow bisects the well-spaced centrosomes; shallow furrows form over closely spaced centrosomes. Time is indicated in minutes:seconds. (D) Long-term differential interference contrast sequence of two halves of a bisected sand dollar zygote. The film began shortly after the unbisected zygote would have divided; because each half has only one centrosome, neither divided at first mitosis. All subsequent divisions proceeded normally in the nucleated half (right), creating a perfect blastula. The anucleate half cleaved abortively in its first attempt. After that, four centrosomes (dots in the 1:51:40 frame) were variously spaced. The second attempt made deep furrows between the widely separated asters, but none between the closely spaced pair. Subsequent divisions were variously successful. Time is indicated in hours:minutes:seconds. (E) Aster separation strongly correlates to the furrow extent. See Materials and methods for measurement. Video 6 corresponds to A–C.

anaphase (e.g., Fig. 8 A), as confirmed by conducting ablations in cells coexpressing EMTB-3G and mC-H2B (Fig. S5 B and Video 8). Ablation of a single centrosome in metaphase consistently shifted furrows from the spindle midzone toward the ablated pole (Fig. 8, Video 7, and Fig. S5). If the aster regrew substantially, or if the ablation took place in anaphase, no displacement of the furrow resulted (see Fig. S5 C). Partial ablations, in which some microtubules regrew from the irradiated pole, led to modest displacement. Complete ablations caused cells to establish furrows that closed near (Fig. 8, A, B, and D) or beyond (Fig. S5, A and C) the ablated aster, often partitioning both chromosome sets into the daughter cell with an intact centrosome. In most singly ablated cells, furrowing completed without significant attempts by the cell to correct furrow position; this contrasts with the results of physical spindle displacement (Bement et al., 2005) or TSA treatment (this paper).

We also conducted ablations in cells coexpressing GFP-rGBD with 3C-EMTB. Because of numerous experimental factors (see Materials and methods), double labeling was often faint. Even so, some crucial observations emerged: first, Rho zones appeared even in cells with extreme ablations; second,

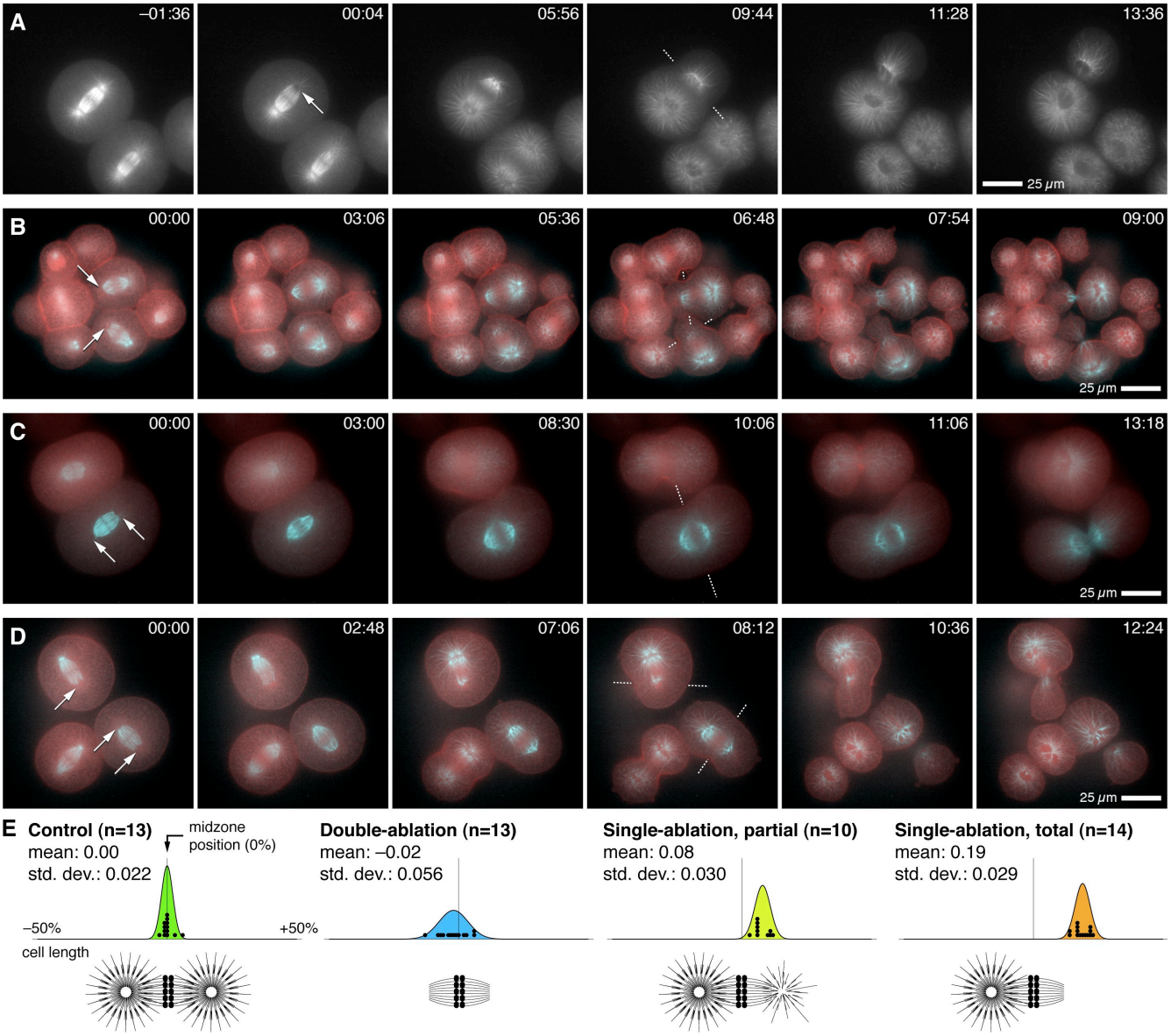

Figure 8. **Centrosome ablation displaces furrows.** (A–D) Single-plane recordings of sand dollar embryos expressing EMTB-3G alone (A) or GFP-rGBD (red) and 3C-EMTB (cyan; B–D); time is shown in minutes:seconds after last irradiation. Arrows, ablation sites; dotted lines, furrow plane. (A) Single-pole ablation in a moderately large cell. Few astral microtubules remain; furrowing occurs over the spindle end rather than the midzone (see Video 7). (B) Two single-pole ablations. Furrows form over and close upon the ablated end. In the top cell, chromosomes are partitioned by the furrow; in the bottom cell, they are not. Rho activity zones in ablated cells are similar to normal cells but shifted. (C) Double-pole ablation in a large cell. A broad furrow with barely detectable Rho activity forms above the spindle midplane and closes between spindle halves. (D) A normal cell (left), singly ablated cell (top), and doubly ablated cell (right). The furrow in the doubly ablated cell is broad, with dilute Rho activity, but closes accurately. The furrow in the singly ablated cell is shifted away from the midplane. (E) Distances (percentage of cell length) between spindle midplane and furrow plane in control, double-, and single-ablated cells (dots) superimposed upon normal curves computed from mean and standard deviation. Video 9 corresponds to B–D.

these zones were not notably different (broader, brighter, or dimmer) than zones in normal cells (Fig. 8 B and Video 9); and third, rather than appearing asymmetrically (as one would expect if asters only inhibited Rho activation), zones were centered on the eventual furrow site. Importantly, we did not find more Rho activity than normal on the polar cortex near ablated centrosomes, which implies that asters or centrosomes shape the distribution of the cytokinetic signal rather than only inhibiting it; if the latter were true, we would expect Rho activation to take place in a normal spatial relation to the intact centrosome instead of shifting distally, as we observed.

We also ablated both centrosomes, which was difficult given the narrow time window and the likelihood of missing one or both poles. In several instances, we accomplished this operation with minimal aster regrowth and without preventing anaphase (Fig. 8, C and D; and Fig. S5 B). In some doubly ablated cells that executed anaphase, cleavage failed, and cells exhibited only incoherent surface ruffling. Other doubly ablated cells initiated broad, shallow furrows, approximately over the midzone (Fig. 8 C). Many of these completed cytokinesis, often (not always) partitioning daughter chromosomes to daughter cells (compare two doubly ablated cells in Fig. S5 B).

This is consistent with results from TSA treatment, collectively implying that asters confer accuracy and precision to the cytokinetic signaling mechanism. To quantify this we scored all centrosome-ablated, EMTB-expressing cells that made credible attempts at cleavage into three categories: double ablations, partial single-pole ablations, and total single-pole ablations. In each, and in controls from the same films, we measured the concurrence of furrow plane and spindle midzone, normalized by cell diameter. The results, superimposed upon normal curves computed from mean and variance in each category (Fig. 8 E), show that doubly ablated cells are less precise than controls but accurate in aggregate, whereas singly ablated cells are precisely inaccurate.

Discussion

Our most surprising finding is that astral microtubules are not needed to transmit the cytokinetic signal, even in large round cells where the nearest spindle microtubule is far from the cell surface. Although it could be argued that our experimental approaches account for this result, the EMTB probes reveal both dynamic and stable microtubules, and precisely colocalize with all astral and cortical microtubules revealed by anti-tubulin in fixed samples. The cortical distribution of microtubules seen in living cells with EMTB parallels that detected by careful EM analysis of urchin zygotes (Asnes and Schroeder, 1979). Thus, if there is some significant cortical microtubule population not detected by EMTB-based probes, it is also undetectable by any other means currently available. Moreover, the same results are obtained in fixed samples never microinjected with EMTB nor subjected to live imaging, and the TSA results are supported by those obtained with nocodazole. Collectively, these results compel the conclusion that neither astral microtubules extending from centrosomes to regions outside the equator, astral microtubules extending from centrosomes to the equator, nor microtubules extending from the midzone to the equator are necessary for delivery of the cytokinetic signal from the spindle to the cortex.

The second finding is that centrosomes, or the asters that grow from them, limit the spatial extent of the cytokinetic signal. This idea is not new, but the approach—centrosome ablation in urchin blastomeres—complements those used in other studies and affirms this principle in urchin embryos. The latter point is critical: it has been vigorously argued, based on micromanipulation studies of urchin zygotes, that asters provide a positive signal that is summed at the equator (for reviews see Rappaport, 1996; Burgess and Chang, 2005). If this were true, ablation of a single centrosome should shift cytokinetic apparatus assembly away from the ablated centrosome. In fact, exactly the opposite happens: the cytokinetic apparatus is displaced toward the ablated centrosome, often so far that all chromosomes end up in one daughter cell. An inhibitory signal from the asters is consistent with studies showing that myosin-powered cortical flow is directed away from microtubule-organizing centers (Hird and White, 1993; Benink et al., 2000; Chen et al., 2008), formation of furrows away from asters during cytokinesis in monopolar cells (Canman et al., 2003; Hu et al., 2008), and local symmetry breaking of a cortical myosin-2 network by displaced asters in *Caenorhabditis elegans* embryos (Werner et al., 2007). However, most of these studies, including ours, posit that this requires direct action of microtubules at the cortex, a presumption challenged by our results.

Asters could limit the cytokinetic cue either by inhibiting that signal locally—by providing an antagonist, by sequestration, or by degradation—or by spatially confining the signal to the equatorial region (e.g., through plus-end-directed transport of the signal or its generators away from the centrosomes). Simple inhibition would predict that the Rho zone would be broader and brighter after destruction of one or both asters, in contrast to what we observed. Instead, the Rho zone is diluted by reduction of the asters with TSA, and ablation of a single centrosome shifts the Rho zone away from the remaining aster without increasing the intensity or breadth. This argues that asters spatially confine the signal, thus enhancing it locally by preventing it from spreading away from the equator.

Our third finding is that although paired asters without a midzone can direct cytokinetic apparatus induction as previously described (Rappaport, 1961), they can do so only under limited geometrical conditions. The use of a live microtubule label reveals unambiguously and for the first time that microtubules from paired asters penetrate the cortex extensively, regardless of whether a furrow forms, and paired asters induce furrows only if there is a microtubule-poor corridor between them. This further argues that the centrosomes or asters limit, rather than create, the cytokinetic signal, as otherwise, closely separated asters would be more potent furrow inducers than distant ones. Anucleate cytoplasts lack chromosomes or midzone but likely retain the molecular species that normally generate the cytokinetic signal. Therefore, if the asters spatially confine the signal rather than simply inhibiting or promoting it, then perhaps juxtaposed asters, in anucleate cytoplasts or toroidal cells, elicit furrowing by concentrating enough of the participants between them.

If the cytokinetic signal can pattern the cortex without the aid of microtubules, how does it get there? Actin can support myosin-powered vectorial transport, but F-actin is dispensable for cytokinetic apparatus specification (Straight et al., 2003; Bement et al., 2005; Foe and von Dassow, 2008). Intermediate filaments and membrane systems permeate the cell but are inherently nonpolar, so it is hard to imagine how they could conduct signals from spindle to cortex. We are led to hypothesize that the primary signal for cytokinesis reaches the cell surface from the spindle by diffusion.

Diffusion seems a poor means to accurately deliver a signal from an interior structure to the cell periphery across large distances, but a diffusible cue arising from the cell interior could be sharpened by at least three nonexclusive mechanisms. First, if the signal is inactivated or sequestered at centrosomes or by astral microtubules (even if they do not reach the cortex), lateral spreading would be suppressed. Centrosomal inactivation could occur by microtubule-independent means as described previously for polarization in *C. elegans* embryos (Cowan and Hyman, 2004). Sequestration could result from microtubule binding by MKLP1 or other candidate signaling agents.

Second, the microtubule-poor corridor between asters could represent a path from the central spindle to the cell surface in which the putative diffusible signal is relatively mobile. Thus, an initial bias established by the spindle in the cell center would be maintained out to the cell surface. If the few microtubules penetrating this region tended to trap potential signal generators (e.g., chromosomal passenger proteins or centralspindlin), such an effect would be enhanced.

Third, an initially broad signal could be sharpened at or near the cortex. A microtubule-independent mechanism is indicated by the fact that Rho zones eventually focus even when microtubules don't reach the cortex, whereas a microtubule-dependent mechanism is suggested because partial inhibition of astral microtubule outgrowth enhances myosin recruitment (Foe and von Dassow, 2008). Anillin, which binds F-actin, Rho, and MgcRacGAP, is a good candidate for the first type of amplifier (e.g., D'Avino et al., 2008); transport of centralspindlin or chromosomal passenger proteins along stable microtubules to the equator (Canman et al., 2003; D'Avino et al., 2006; Odell and Foe, 2008), and inhibition of Rho activation by microtubules outside the equator (Werner et al., 2007; Odell and Foe, 2008; Murthy and Wadsworth, 2008), are good candidates for the second kind of amplifier.

The core proposition—that the primary cytokinetic signal is focused to the equator by the combined action of the spindle midzone and the centrosomes—requires that future attention be directed toward parameters that are not yet well established, such as realistic diffusion and transport rates for large macromolecular complexes (like centralspindlin) over long distances within the cytoplasm, and on distinctions that few studies of cytokinesis have made, i.e., to differentiate the role of the aster from the role of other centrosome-associated cellular constituents.

Materials and methods

Eggs and microinjections

Gametes of the purple urchin *Strongylocentrotus purpuratus* and the sand dollar *Dendraster excentricus* were obtained either by intracoelomic injection of 0.56 M KCl or, for purple urchins, by alternately bouncing then shaking a gravid individual in the palm of the hand. Sperm were collected dry from the aboral surface and kept chilled until use. Purple urchin eggs were shed into a large volume of coarse-filtered seawater (FSW), rinsed twice in FSW, and stored settled at sea-table temperature (11–14°C) until use. Sand dollar eggs were shed into a large volume of FSW and left unrinsed at sea-table temperature until use. All echinoderm embryo culture likewise took place at sea-table temperature.

Purple urchin eggs were prepared for injection by dejellying with two rapid washes in calcium/magnesium-free artificial seawater, then returned to FSW in dishes rendered nonsticky by washing with 1% BSA in FSW. Dejellied eggs were used within 2 h. For injections, coverslip-bottom dishes were coated by washing 30 s in 1% protamine sulfate, rinsing 3× in distilled water, and air drying. Dejellied purple urchin eggs were arranged in a row in an injection dish filled with FSW + 1 mM 3-aminotriazole, which prevents hardening of the vitelline envelope, then fertilized by addition of several drops of a 1:10,000 dilution of dry sperm. Good batches of gametes yield nearly 100% fertilization within 5 min. For imaging, purple urchin embryos were removed from their still-soft vitelline envelopes using a hand-pulled mouth pipet, and transferred either directly to a microscope slide or into to a plastic Petri dish coated with 1% BSA in FSW.

Sand dollar eggs were fertilized within their jelly by the addition of 1–2 ml of sperm diluted ~1:10,000 in FSW. 10–15 min after insemination, fertilized eggs were deprived of their jelly and vitelline envelopes by one passage in and out of a hand-pulled mouth pipet cut to slightly larger than the egg diameter. To prevent stripped eggs from sticking to glass, culture vessels were coated with 1% BSA in FSW before adding eggs. For injection, stripped sand dollar eggs were arranged in a row in an uncoated coverslip-bottom dish that had been cleaned with 95% ethanol. Clean glass is sticky enough to enable microinjection but allow release of injected embryos with gentle swirling.

Both species of urchin eggs were injected with 0.5–2% of the cell volume (a sand dollar egg is ~1 nl; a purple urchin egg is ~0.3 nl) using needles made from 1 mm OD filament-containing capillaries on a micropipette puller (P-97; Sutter Instrument Co.). Injections were performed on an inverted microscope (TS100; Nikon) equipped with a cooling stage (Dagan Corporation) maintained at 12°C, using a hanging-joystick oil hydraulic micromanipulator (Narishige) and Picospritzer III (Parker Hannifin Corp.). Needle concentration of RNA was 1 ng/nl or less for GFP-rGBD or mC-H2B, and <0.1 ng/nl for EMTB-3G and 3C-EMTB. We found that injection of higher levels of EMTB-based probes caused increasingly severe early defects, including mitotic spindle bifurcation, due apparently to a delay in metaphase during which duplicated centrosomes prematurely separate or, at the highest levels, complete cell cycle arrest (Fig. S1 A). Notably, for both purple urchins and sand dollars, normal embryos that develop from zygotes injected with 0.05–0.1 ng/nl EMTB-3G mRNA are many times brighter by the 32-cell stage than are the usually defective four- and eight-cell embryos that result from injection of higher levels. We therefore surmise that either the earliest cell divisions are especially sensitive to the introduction of an exogenous microtubule-binding moiety or that rapid expression of this probe cannot be tolerated (perhaps because some slow posttranslational modification renders it less harmful). Therefore, all results reported here on purple urchins and sand dollars come from eight-cell embryos and beyond, injected with a dose of mRNA at which mitotic defects were rare.

X. laevis embryos were obtained and injected as described previously (Bement et al., 2005). Each blastomere of the two-cell embryo was injected with 5 nl of either EMTB-3G mRNA alone (0.01–0.04 ng/nl) or 5 nl of a mixture of 3C-EMTB and GFP-rGBD at final needle concentrations of 0.04 and 0.2 ng/nl, respectively.

Constructs and mRNA synthesis

All constructs were assembled in pCS2 modified to contain three EGFP at the putative carboxy terminus, or one or three mCherry at the amino terminus. mRNA was synthesized from linearized plasmids using the SP6 mMessage mMachine kit (Applied Biosystems), according to the manufacturer's instructions.

Live imaging and drug perfusion

Sand dollar or purple urchin embryos were placed on a clean glass slide in a 10–20 µl drop of FSW, between two ridges of high vacuum grease (Dow Corning) spaced ~1 cm apart. A coverslip was applied, resting on the grease ridges, and then pressed down until eggs or embryos were trapped by slight-to-moderate compression. With some batches of eggs, we found it necessary to coat slides and coverslips by rinsing with 1% BSA in FSW to prevent cells from sticking too tightly to the glass and thus deforming themselves during cytokinesis. These chambers remained open on both ends, allowing perfusion of solutions by addition of large drop (40–50 µl) of FSW containing either nocodazole or TSA and up to 0.1% DMSO.

Purple urchin and sand dollar embryos were imaged with a laser scanning confocal microscope (Radiance 2000; Bio-Rad Laboratories) mounted on a compound microscope (E800; Nikon) using a 40× 1.3 NA Plan-Fluor oil lens. Room temperature was maintained at 14–17°C, which is tolerated well by both species. Some experiments were conducted on a spinning disc confocal microscope (CARV; BD) consisting of an inverted microscope (TE2000; Nikon) with a 60× 1.4 NA Plan-Apochromat oil lens and a 60× 1.2 NA Plan-Apochromat water lens, the CARV spinning disc head, and a camera (ORCA-ER; Hamamatsu), controlled by MetaMorph software (MDS Analytical Technologies). *X. laevis* embryos were imaged on a laser scanning confocal microscope (1024; Bio-Rad Laboratories) mounted on an Axiovert microscope (Carl Zeiss, Inc.) using a 63× 1.4 NA Plan-Apochromat oil objective.

Fixation and antibody staining

Embryos were fixed by transferring 200–300 devitellinized sand dollar embryos in 100 µl of seawater into 900 µl of fixative at a final concentration of 2% formaldehyde (from 20% EM-grade stock), 0.2% glutaraldehyde, 0.2% Triton X-100, 100 mM Hepes, pH 7.0, 50 mM EGTA, 10 mM $MgSO_4$, and 400 mM dextrose. After 1 h in fixative, embryos were rinsed 3× in PBT and once in PBS, treated for 2 h with 0.1% sodium borohydride in PBS (to reduce autofluorescence), washed once in PBS, then blocked in

5% normal goat serum (Jackson ImmunoResearch Laboratories, Inc.), 0.1% BSA in PBT. Embryos were incubated for 24 h at room temperature with 1:1,000 YL1/2 rat anti–α-tubulin (AbD Serotec), 1:500 rabbit anti-GFP (Invitrogen), or 1:500 rabbit anti-phosphoSer19-myosin regulatory light chain (Cell Signaling Technology) in PBT; washed 3× in PBT; incubated for 24 h with 1:500 Alexa Fluor 488 goat anti−rat IgG, Alexa Fluor 488 goat anti–rabbit IgG, Alexa Fluor 568 goat anti–rat IgG, or Alexa Fluor 568 goat anti–rabbit IgG (all from Invitrogen); washed 3× in PBT and 2× in PBS; and mounted in VectaShield medium (Vector Laboratories). Fixed embryos were examined on a laser scanning confocal microscope (FluoView 1000; Olympus) with a 60× 1.4 NA Plan Apochromat oil lens.

Analysis of Rho zone width

As described previously (Bement et al., 2005), single frames from equivalent stages of furrow ingression were selected from sequences at medial planes within cells expressing GFP-rGBD alone or with 3C-EMTB. A freehand line selection was drawn along the cell edge and then straightened using ImageJ. Intensities were plotted along a 7-pixel-wide band covering the cell edge, yielding data points (position and intensity) spanning the Rho zone in the furrow. Intensity data were imported into Mathematica (Wolfram Research, Inc.) and fit with a Gaussian curve plus a quadratic equation with small coefficients. The Gaussian curve fits the Rho zone, whereas the quadratic fits the background cortical signal level. The width of the Rho zone was taken as twice the standard deviation of the fit Gaussian curve, which is equivalent to slightly less than the peak width at half maximum height. Total intensity of the Rho zone was taken as the integral under the Gaussian curve from the center plus or minus two standard deviations, minus the integral in the baseline fit over the same region. Zone widths plotted in Fig. 6 B were normalized by the pole-to-pole distance in each measured cell. Significance was judged using the mean difference test in Mathematica.

Creation and analysis of anucleate cytoplasts

Sand dollar zygotes were bisected either freehand using a fine glass needle or using a needle mounted on a hanging-joystick oil hydraulic micromanipulator (Narishige Group). Bisection was conducted after pronuclear fusion for uninjected eggs, or ∼45 min after fertilization (and after injection) for injected eggs. Bisection yields half zygotes, which by random chance include some pairs in which one half contains the nucleus and a single centrosome and the other half contains only a centrosome. Such pairs were recognized by differential interference contrast microscopy or by staining live cells with Hoechst 33342. Anucleate, centrosome-containing cytoplasts conduct orderly centrosome duplication and separation on a normal schedule; the nucleated half skips first cleavage, then develops normally as a tetraploid (Fig. 8 D). Among EMTB-3G–expressing anucleate cytoplasts, we scored all cases in which either no furrows or discrete furrows formed (omitting cases in which the cytoplast strangled itself into the shape of a balloon animal, which we took to be a sign of poor health) as follows: for each centrosome pair in focus, we measured, at the time corresponding to anaphase, the distance between centrosomes and divided by the distance from the midpoint between them to the cell surface. We then scored cortical behavior into three categories: (1) no furrow or incoherent ruffling, (2) shallow furrow, or (3) deep or complete furrow. Significance was judged using the mean difference test in Mathematica.

Centrosome ablation and analysis

We used a highly focused pulsed UV laser (MicroPoint; Photonic Instruments, Inc.) coupled to an inverted microscope (TE2000) with a CARV spinning disk unit. All ablations were performed on sand dollar embryos using 365-nm light and a 60× 1.25 NA Plan-Fluor oil lens; the suboptimal NA of this lens imposes a nearly twofold cost in image brightness, but the higher UV transmittance was found to be essential. Double labeling (as in Fig. 8, B–D) further required a double band GFP/dsRed filter set (Chroma Technology Corp.), which imposes a further twofold cost in brightness. To destroy a centrosome in metaphase, as judged by collapse of the aster around it, required rapid pulses (10–20 Hz) at full power over several seconds. This amount of irradiation bleached GFP-based probes by as much as twofold per successful centrosome destruction. Our frequent misses constituted a built-in control: cells subjected to this degree of cytoplasmic irradiation outside the spindle suffered no ill effects (beyond bleaching). We found it difficult, though not impossible, to perform similar ablations in purple urchin embryos, as they are substantially more opaque than sand dollar embryos. Ablated cells and controls from the same recordings were analyzed using ImageJ by making three measurements: the pole-to-pole cell length, the midpoint between the spindle ends (not poles, as one or both were destroyed), and the position of the furrow. The latter was measured by drawing a line from the inflection point of the curved cell surface during midfurrow ingression to the inflection point on the opposite side, and measuring the intersection with a line drawn along the spindle axis. Data were plotted and tested for significance in Mathematica.

Image processing

3D projection of confocal z series (brightest-point projection only; no volume rendering) and measurements from time-lapse confocal data were conducted using ImageJ. Images were adjusted for white and black point; no gamma adjustment or nonlinear filtering was applied except as noted in the figure legends. Kymographs were created from time-lapse sequences using ImageJ (Fig. S1 D′ and Fig. 2 B) or the freeware volume rendering program Voxx (http://www.nephrology.iupui.edu/imaging/voxx/; Fig. 2, A′ and C). Fig. 2 A was made using a brightest-point projection, and Fig. 2 C by using α blending such that only the surface is visible. Pseudocoloring and figure layout were performed in ImageJ or Photoshop CS3 (Adobe).

Online supplemental material

Fig. S1 demonstrates the viability of urchin embryos expressing EMTB-3G and documents cortical microtubule dynamics in *X. laevis* embryos. Fig. S2 displays colocalization between EMTB-3G and anti-tubulin in fixed sand dollar embryos. Fig. S3 contrasts microtubule configuration in normal and TSA-treated urchin embryos expressing both EMTB-3G and mC-H2B. Fig. S4 presents extreme cases of TSA treatment. Fig. S5 presents additional cases of centrosome-ablated cells. Video 1 shows EMTB-3G in normal purple urchin and sand dollar embryos. Video 2 corresponds to Fig. S1 D: superficial view of EMTB-3G in normal *X. laevis* blastomere. Video 3 shows nocodazole-treated purple urchin and sand dollar embryos expressing EMTB-3G. Video 4 shows TSA-treated purple urchin and sand dollar embryos expressing EMTB-3G. Video 5 shows untreated and TSA-treated purple urchin embryos expressing EMTB-3G and mC-H2B. Video 6 shows anucleate sand dollar cytoplasts expressing EMTB-3G. Video 7 shows sand dollar blastomeres expressing EMTB-3G, in which a single centrosome was ablated in metaphase. Video 8 shows sand dollar embryo expressing EMTB-3G and mC-H2B, in which two cells suffered ablation of both centrosomes in metaphase, and two cells experienced ablation of a single pole. Video 9 shows centrosome-ablated sand dollar blastomeres expressing GFP-rGBD and 3C-EMTB. Online supplemental material is available at http://www.jcb.org/cgi/content/full/jcb.200907090/DC1.

This paper was supported by National Institutes of Health grant GM066050 to G.M. Odell and grant GM052932 to W.M. Bement, National Science Foundation grant MCB-0917887 to G. von Dassow, and a Michael Guyer Fellowship to K. J.C. Verbrugghe.

Submitted: 16 July 2009
Accepted: 16 November 2009

References

Adams, R.R., A.A. Tavares, A. Salzberg, H.J. Bellen, and D.M. Glover. 1998. pavarotti encodes a kinesin-like protein required to organize the central spindle and contractile ring for cytokinesis. *Genes Dev.* 12:1483–1494. doi:10.1101/gad.12.10.1483

Asnes, C.F., and T.E. Schroeder. 1979. Cell cleavage. Ultrastructural evidence against equatorial stimulation by aster microtubules. *Exp. Cell Res.* 122:327–338. doi:10.1016/0014-4827(79)90309-4

Baruni, J.K., E.M. Munro, and G. von Dassow. 2008. Cytokinetic furrowing in toroidal, binucleate and anucleate cells in *C. elegans* embryos. *J. Cell Sci.* 121:306–316. doi:10.1242/jcs.022897

Beams, H.W., and T.C. Evans. 1940. Some effects of colchicines upon the first cleavage in *Arbacia punctulata*. *Biol. Bull.* 79:188–198. doi:10.2307/1537838

Belmont, L.D., A.A. Hyman, K.E. Sawin, and T.J. Mitchison. 1990. Real-time visualization of cell cycle-dependent changes in microtubule dynamics in cytoplasmic extracts. *Cell.* 62:579–589. doi:10.1016/0092-8674(90)90022-7

Bement, W.M., H.A. Benink, and G. von Dassow. 2005. A microtubule-dependent zone of active RhoA during cleavage plane specification. *J. Cell Biol.* 170:91–101. doi:10.1083/jcb.200501131

Benink, H.A., and W.M. Bement. 2005. Concentric zones of active RhoA and Cdc42 around single cell wounds. *J. Cell Biol.* 168:429–439. doi:10.1083/jcb.200411109

Benink, H.A., C.A. Mandato, and W.M. Bement. 2000. Analysis of cortical flow models in vivo. *Mol. Biol. Cell.* 11:2553–2563.

Birkenfeld, J., P. Nalbant, B.P. Bohl, O. Pertz, K.M. Hahn, and G.M. Bokoch. 2007. GEF-H1 modulates localized RhoA activation during cytokinesis under the control of mitotic kinases. *Dev. Cell.* 12:699–712. doi:10.1016/j.devcel.2007.03.014

Bringmann, H., and A.A. Hyman. 2005. A cytokinesis furrow is positioned by two consecutive signals. *Nature.* 436:731–734. doi:10.1038/nature03823

Burgess, D.R., and F. Chang. 2005. Site selection for the cleavage furrow at cytokinesis. *Trends Cell Biol.* 15:156–162. doi:10.1016/j.tcb.2005.01.006

Bütschli, O. 1876. Studien uber die ersten Entwicklungsvorgange der Eizelle, die Zelltheilung und die Conjugation der Infusorien. Abhandlungen, Herausgegeben von der Senckenbergischen. *Naturforschenden Gesellschaft*, 10:213-464.

Canman, J.C., L.A. Cameron, P.S. Maddox, A. Straight, J.S. Tirnauer, T.J. Mitchison, G. Fang, T.M. Kapoor, and E.D. Salmon. 2003. Determining the position of the cell division plane. *Nature.* 424:1074–1078. doi:10.1038/nature01860

Chen, W., M. Foss, K.F. Tseng, and D. Zhang. 2008. Redundant mechanisms recruit actin into the contractile ring in silkworm spermatocytes. *PLoS Biol.* 6:e209. doi:10.1371/journal.pbio.0060209

Cowan, C.R., and A.A. Hyman. 2004. Centrosomes direct cell polarity independently of microtubule assembly in *C. elegans* embryos. *Nature.* 431:92–96. doi:10.1038/nature02825

D'Avino, P.P., M.S. Savoian, L. Capalbo, and D.M. Glover. 2006. RacGAP50C is sufficient to signal cleavage furrow formation during cytokinesis. *J. Cell Sci.* 119:4402–4408. doi:10.1242/jcs.03210

D'Avino, P.P., T. Takeda, L. Capalbo, W. Zhang, K.S. Lilley, E.D. Laue, and D.M. Glover. 2008. Interaction between Anillin and RacGAP50C connects the actomyosin contractile ring with spindle microtubules at the cell division site. *J. Cell Sci.* 121:1151–1158. doi:10.1242/jcs.026716

Dechant, R., and M. Glotzer. 2003. Centrosome separation and central spindle assembly act in redundant pathways that regulate microtubule density and trigger cleavage furrow formation. *Dev. Cell.* 4:333–344. doi:10.1016/S1534-5807(03)00057-1

Devore, J.J., G.W. Conrad, and R. Rappaport. 1989. A model for astral stimulation of cytokinesis in animal cells. *J. Cell Biol.* 109:2225–2232. doi:10.1083/jcb.109.5.2225

Faire, K., C.M. Waterman-Storer, D. Gruber, D. Masson, E.D. Salmon, and J.C. Bulinski. 1999. E-MAP-115 (ensconsin) associates dynamically with microtubules in vivo and is not a physiological modulator of microtubule dynamics. *J. Cell Sci.* 112:4243–4255.

Foe, V.E., and G. von Dassow. 2008. Stable and dynamic microtubules coordinately shape the myosin activation zone during cytokinetic furrow formation. *J. Cell Biol.* 183:457–470. doi:10.1083/jcb.200807128

Hamaguchi, Y. 1975. Microinjection of colchicines into sea urchin eggs. *Dev. Growth Differ.* 17:111–117. doi:10.1111/j.1440-169X.1975.00111.x

Harris, P. 1961. Electron microscope study of mitosis in sea urchin blastomeres. *J. Biophys. Biochem. Cytol.* 11:419–431.

Harris, A.K., and S.L. Gewalt. 1989. Simulation testing of mechanisms for inducing the formation of the contractile ring in cytokinesis. *J. Cell Biol.* 109:2215–2223. doi:10.1083/jcb.109.5.2215

Hiramoto, Y. 1956. Cell division without mitotic apparatus in sea urchin eggs. *Exp. Cell Res.* 11:630–636. doi:10.1016/0014-4827(56)90171-9

Hird, S.N., and J.G. White. 1993. Cortical and cytoplasmic flow polarity in early embryonic cells of *Caenorhabditis elegans*. *J. Cell Biol.* 121:1343–1355. doi:10.1083/jcb.121.6.1343

Hu, C.K., M. Coughlin, C.M. Field, and T.J. Mitchison. 2008. Cell polarization during monopolar cytokinesis. *J. Cell Biol.* 181:195–202. doi:10.1083/jcb.200711105

Inoue, Y.H., M.S. Savoian, T. Suzuki, E. Máthé, M.T. Yamamoto, and D.M. Glover. 2004. Mutations in orbit/mast reveal that the central spindle is comprised of two microtubule populations, those that initiate cleavage and those that propagate furrow ingression. *J. Cell Biol.* 166:49–60. doi:10.1083/jcb.200402052

Kamijo, K., N. Ohara, M. Abe, T. Uchimura, H. Hosoya, J.S. Lee, and T. Miki. 2006. Dissecting the role of Rho-mediated signaling in contractile ring formation. *Mol. Biol. Cell.* 17:43–55. doi:10.1091/mbc.E05-06-0569

Mandato, C.A., H.A. Benink, and W.M. Bement. 2000. Microtubule-actomyosin interactions in cortical flow and cytokinesis. *Cell Motil. Cytoskeleton.* 45:87–92. doi:10.1002/(SICI)1097-0169(200002)45:2<87::AID-CM1>3.0.CO;2-0

Matsuyama, A., T. Shimazu, Y. Sumida, A. Saito, Y. Yoshimatsu, D. Seigneurin-Berny, H. Osada, Y. Komatsu, N. Nishino, S. Khochbin, et al. 2002. In vivo destabilization of dynamic microtubules by HDAC6-mediated deacetylation. *EMBO J.* 21:6820–6831. doi:10.1093/emboj/cdf682

Minestrini, G., A.S. Harley, and D.M. Glover. 2003. Localization of Pavarotti-KLP in living *Drosophila* embryos suggests roles in reorganizing the cortical cytoskeleton during the mitotic cycle. *Mol. Biol. Cell.* 14:4028–4038. doi:10.1091/mbc.E03-04-0214

Motegi, F., N.V. Velarde, F. Piano, and A. Sugimoto. 2006. Two phases of astral microtubule activity during cytokinesis in *C. elegans* embryos. *Dev. Cell.* 10:509–520. doi:10.1016/j.devcel.2006.03.001

Murthy, K., and P. Wadsworth. 2008. Dual role for microtubules in regulating cortical contractility during cytokinesis. *J. Cell Sci.* 121:2350–2359. doi:10.1242/jcs.027052

Nishimura, Y., and S. Yonemura. 2006. Centralspindlin regulates ECT2 and RhoA accumulation at the equatorial cortex during cytokinesis. *J. Cell Sci.* 119:104–114. doi:10.1242/jcs.02737

Odell, G.M., and V.E. Foe. 2008. An agent-based model contrasts opposite effects of dynamic and stable microtubules on cleavage furrow positioning. *J. Cell Biol.* 183:471–483. doi:10.1083/jcb.200807129

Powers, J., O. Bossinger, D. Rose, S. Strome, and W. Saxton. 1998. A nematode kinesin required for cleavage furrow advancement. *Curr. Biol.* 8:1133–1136. doi:10.1016/S0960-9822(98)70470-1

Rappaport, R. 1961. Experiments concerning the cleavage stimulus in sand dollar eggs. *J. Exp. Zool.* 148:81–89. doi:10.1002/jez.1401480107

Rappaport, R. 1986. Establishment of the mechanism of cytokinesis in animal cells. *Int. Rev. Cytol.* 105:245–281. doi:10.1016/S0074-7696(08)61065-7

Rappaport, R. 1996. *Cytokinesis in Animal Cells*. Cambridge University Press, New York. 386 pp.

Saint, R., and W.G. Somers. 2003. Animal cell division: a fellowship of the double ring? *J. Cell Sci.* 116:4277–4281. doi:10.1242/jcs.00816

Schroeder, T.E. 1981. The origin of cleavage forces in dividing eggs. A mechanism in two steps. *Exp. Cell Res.* 134:231–240. doi:10.1016/0014-4827(81)90480-8

Shannon, K.B., J.C. Canman, C. Ben Moree, J.S. Tirnauer, and E.D. Salmon. 2005. Taxol-stabilized microtubules can position the cytokinetic furrow in mammalian cells. *Mol. Biol. Cell.* 16:4423–4436. doi:10.1091/mbc.E04-11-0974

Somers, W.G., and R. Saint. 2003. A RhoGEF and Rho family GTPase-activating protein complex links the contractile ring to cortical microtubules at the onset of cytokinesis. *Dev. Cell.* 4:29–39. doi:10.1016/S1534-5807(02)00402-1

Straight, A.F., A. Cheung, J. Limouze, I. Chen, N.J. Westwood, J.R. Sellers, and T.J. Mitchison. 2003. Dissecting temporal and spatial control of cytokinesis with a myosin II inhibitor. *Science.* 299:1743–1747. doi:10.1126/science.1081412

Strickland, L.I., Y. Wen, G.G. Gundersen, and D.R. Burgess. 2005a. Interaction between EB1 and p150glued is required for anaphase astral microtubule elongation and stimulation of cytokinesis. *Curr. Biol.* 15:2249–2255. doi:10.1016/j.cub.2005.10.073

Strickland, L.I., E.J. Donnelly, and D.R. Burgess. 2005b. Induction of cytokinesis is independent of precisely regulated microtubule dynamics. *Mol. Biol. Cell.* 16:4485–4494. doi:10.1091/mbc.E05-04-0305

Vale, R.D., J.A. Spudich, and E.R. Griffis. 2009. Dynamics of myosin, microtubules, and Kinesin-6 at the cortex during cytokinesis in *Drosophila* S2 cells. *J. Cell Biol.* 186:727–738. doi:10.1083/jcb.200902083

Verbrugghe, K.J., and J.G. White. 2007. Cortical centralspindlin and G alpha have parallel roles in furrow initiation in early *C. elegans* embryos. *J. Cell Sci.* 120:1772–1778. doi:10.1242/jcs.03447

von Dassow, G. 2009. Concurrent cues for cytokinetic furrow induction in animal cells. *Trends Cell Biol.* 19:165–173. doi:10.1016/j.tcb.2009.01.008

Werner, M., E.M. Munro, and M. Glotzer. 2007. Astral signals spatially bias cortical myosin recruitment to break symmetry and promote cytokinesis. *Curr. Biol.* 17:1286–1297. doi:10.1016/j.cub.2007.06.070

White, J.G., and G.G. Borisy. 1983. On the mechanisms of cytokinesis in animal cells. *J. Theor. Biol.* 101:289–316. doi:10.1016/0022-5193(83)90342-9

Wolpert, L. 1960. The mechanics and mechanism of cleavage. *Int. Rev. Cytol.* 10:163–216.

Wright, B.D., M. Terasaki, and J.M. Scholey. 1993. Roles of kinesin and kinesin-like proteins in sea urchin embryonic cell division: evaluation using antibody microinjection. *J. Cell Biol.* 123:681–689. doi:10.1083/jcb.123.3.681

Yoshigaki, T. 1999. Simulation of density gradients of astral microtubules at cell surface in cytokinesis of sea urchin eggs. *J. Theor. Biol.* 196:211–224. doi:10.1006/jtbi.1998.0835

Yüce, O., A. Piekny, and M. Glotzer. 2005. An ECT2-centralspindlin complex regulates the localization and function of RhoA. *J. Cell Biol.* 170:571–582. doi:10.1083/jcb.200501097

Zhao, W.M., and G. Fang. 2005. MgcRacGAP controls the assembly of the contractile ring and the initiation of cytokinesis. *Proc. Natl. Acad. Sci. USA.* 102:13158–13163. doi:10.1073/pnas.0504145102

Published

von Dassow et al., http://www.jcb.org/cgi/content/full/jcb.200907090/DC1

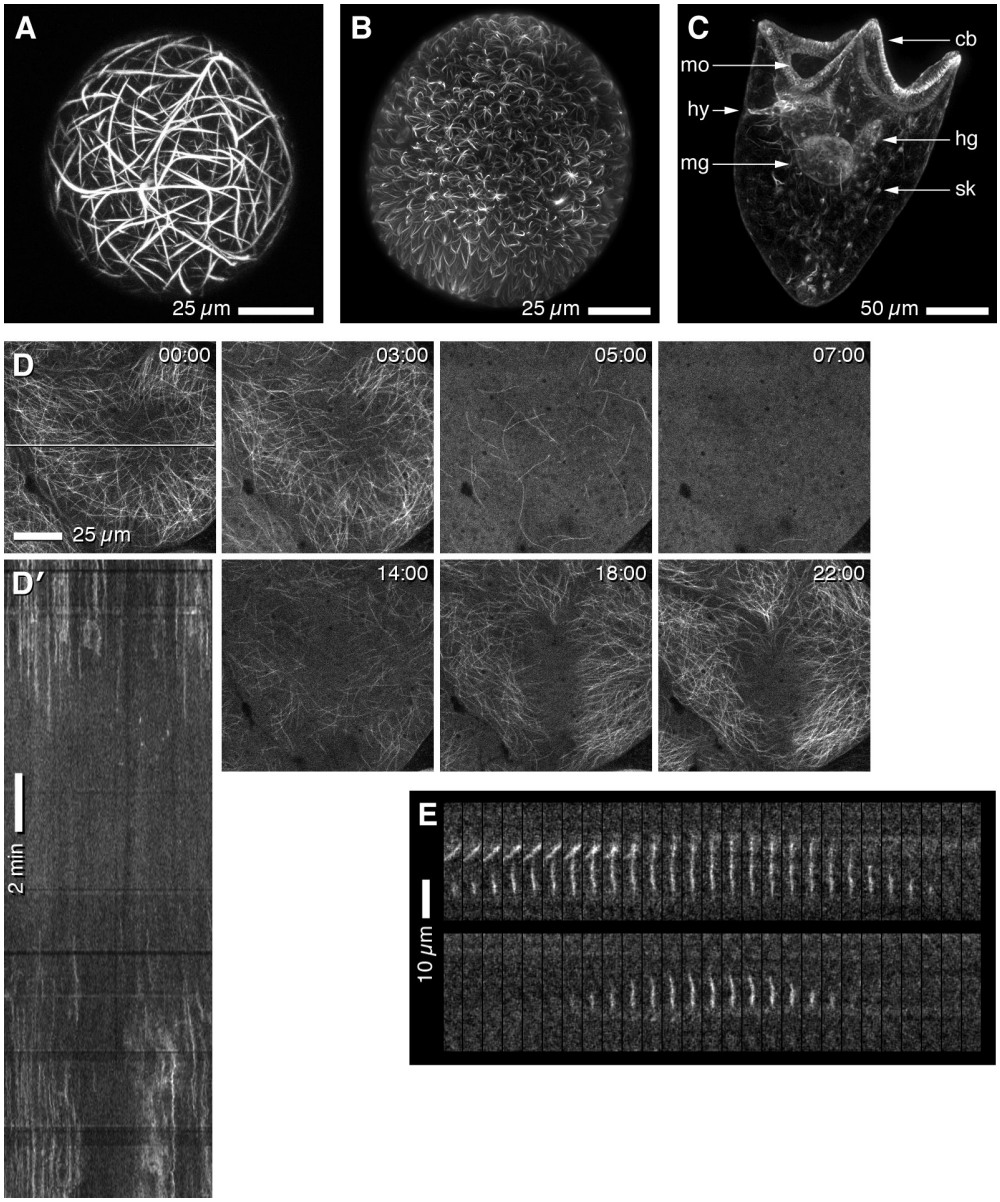

Figure S1. **Moderate expression of EMTB-3G does not interfere with mitosis or morphogenesis.** (A) Purple urchin zygote injected to ~2% egg volume with high concentration (1 ng/nl; >10× normal imaging concentration) EMTB-3G mRNA arrests as a zygote with highly stable microtubule bundles. (B) Projection of 68 0.5-µm confocal sections through a 30-h-old purple urchin embryo at the mesenchyme blastula stage from a zygote injected to ~2% egg volume with normal imaging concentration (0.05 ng/nl) EMTB-3G mRNA. Uniform cell size and consistent apical-basal orientation indicate the scarcity of mitotic or developmental errors. (C) Projection of 44 2-µm sections through a 4-d-old purple urchin pluteus larva, compressed between slide and coverslip to trap it, from the same batch of injected eggs as B. Morphogenesis and relative proportions of ciliated band (cb), skeleton (sk), digestive tract (mo, mouth; mg, midgut; hg, hindgut), and coeloms (hy, hydropore) are all normal. (D) Single superficial sections from a 6 h *X. laevis* embryo (EMTB-3G; Video 2). (D′) Kymograph from single-pixel strip shown in the 00:00 frame of D; as in urchins (Fig. 2), long streaks (kinematically stable microtubules) appear before furrowing, mostly outside the equator. Time is shown in minutes:seconds. (E) Successive frames showing cortical microtubules growing and shrinking (3 s intervals); enlargement from a *X. laevis* blastomere expressing EMTB-3G (intensities squared to enhance contrast).

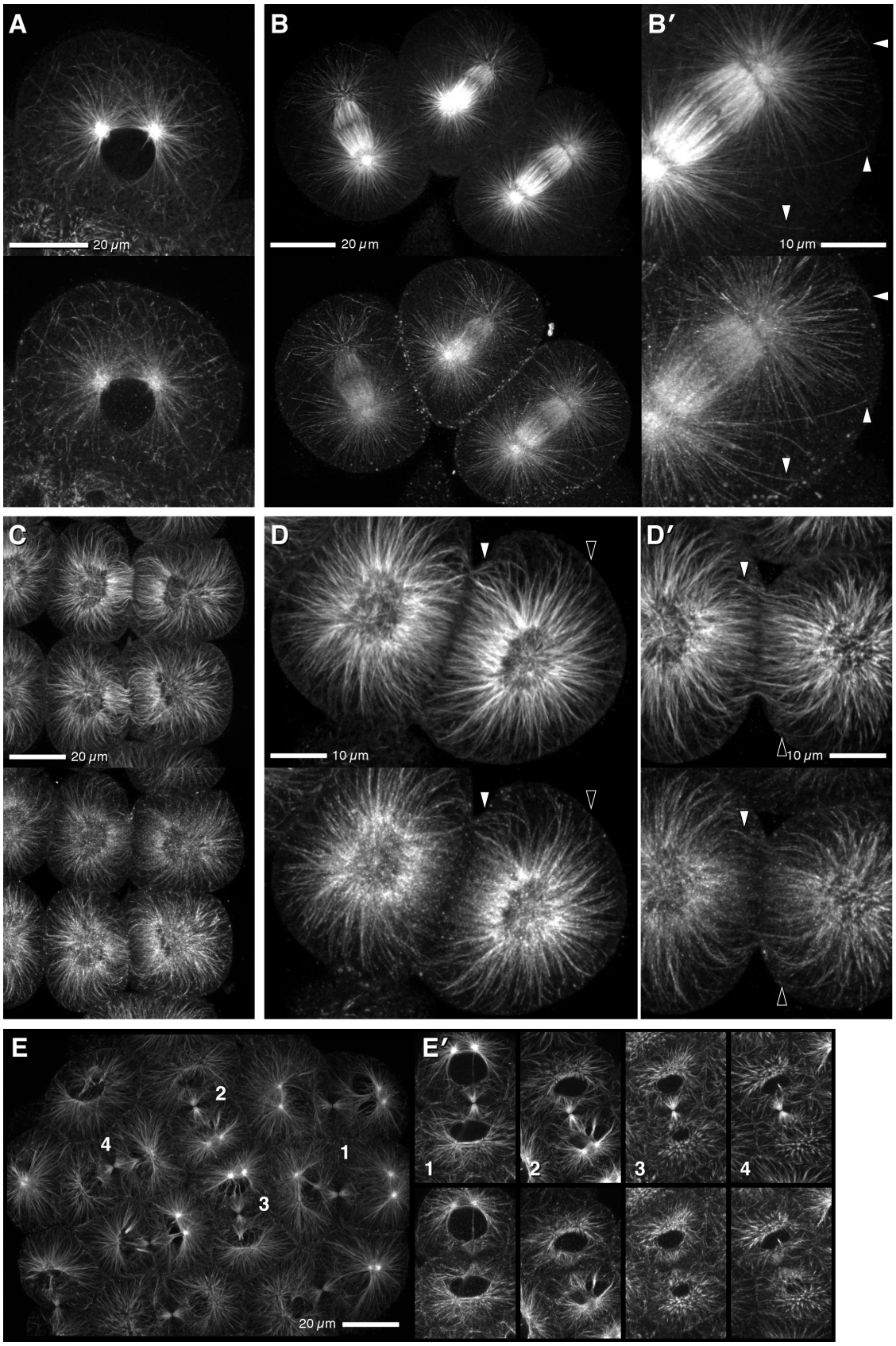

Figure S2. **EMTB-3G colocalizes with microtubules labeled by immunofluorescence.** Sand dollar eggs were injected with <0.05 ng/nl EMTB-3G mRNA, then fixed and labeled with anti-tubulin (top) and anti-GFP (bottom) antibodies. (A) An interphase cell; projection of five 0.3-μm sections. (B and B′) A trio of anaphase cells; projection of 46 0.25-μm sections. B′ shows a 2× enlarged view. Astral microtubules are equally labeled by anti-GFP and anti-tubulin. Note the accurate labeling of apparently single astral microtubules by EMTB-3G (B′, arrowheads). (C and C′) Telophase; projection of five 0.5-μm confocal

sections. Astral microtubules that are collected together by the cleavage furrow, destined for the central spindle, are accurately labeled by EMTB-3G. Midzone microtubules, however, are relatively underlabeled. (D and D′) Two telophase cells from the same embryo; projection of five 0.5-µm confocal sections. Similar to C and C′, astral microtubules gathered together by the ingressing furrow, which will contribute to the midbody, are labeled accurately by EMTB-3G (closed arrowheads), but the midzone of the central spindle is relatively poorly labeled. Open arrowheads point out close correspondence of both labels for astral microtubule ends outside the furrow. (E and E′) Complete cytokinesis. E is a projection of 22 0.5-µm confocal sections (anti-tubulin only), whereas each vertical pair in E′ is a projection of the three sections that include the midbody for each of four cell pairs in E (numbered). The midbody is the brightest object recognized by anti-tubulin besides the centrosomes themselves (E′, top); although most of the midbody is labeled by EMTB-3G (E′, bottom), the very middle is absent, and the midbody as a whole is less brightly labeled than the rest of the microtubule array.

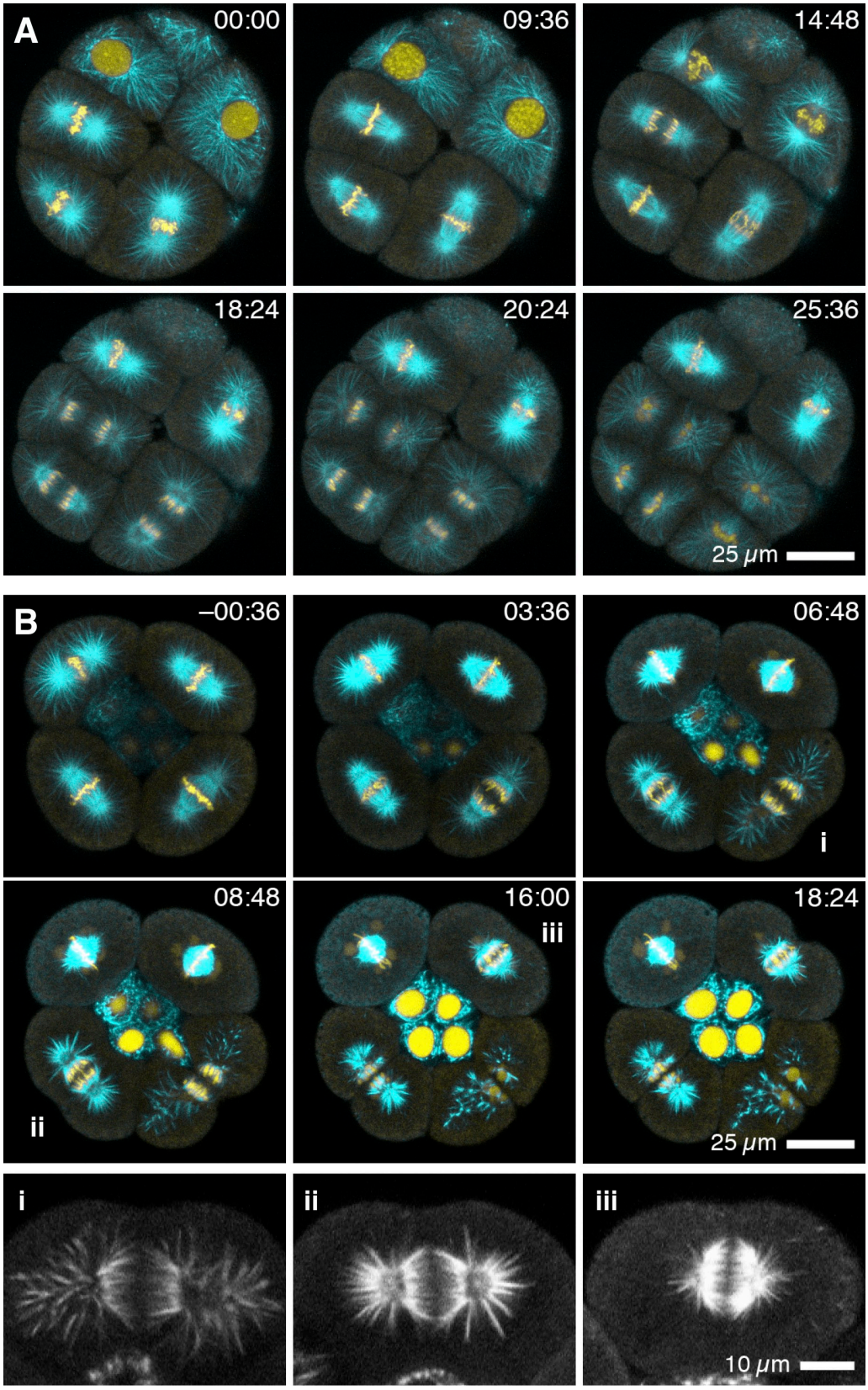

Figure S3. **Accurate cleavage between separating chromatids in control and TSA-treated cells.** Single confocal sections. Cyan, EMTB-3G; yellow, mC-H2B (see Video 5). (A) Untreated 16-cell purple urchin embryo, side view, epitomizing normal correlation between aster development, furrowing, and the extent of separation of sister chromatids. (B) 16-cell purple urchin embryo; 15 μM TSA was added at time 00:00. Because of a slight asynchrony in mitosis at the time of TSA addition, each macromere exhibits a distinct phenotype: the northwest cell has not quite achieved chromosome alignment at the time of TSA addition, and remained in metaphase. Cells that cleaved are shown as 2× enlargements (i–iii). The southeast cell (i) entered anaphase shortly after TSA addition; this cell retained substantial asters with rays that approach, if not reach, the cell surface, and separated sister chromatids significantly. The southwest cell (ii) entered anaphase ~5 min after TSA addition; asters are present but much reduced and do not reach the cortex, and chromatid separation is limited. The northeast cell (iii) entered anaphase 10–12 min after TSA addition, and has both minimal asters and minimal chromatid separation. All three cells that entered anaphase, however, despite differences in aster extent and sister chromatid separation, initiated furrowing at the appropriate position and time after anaphase onset.

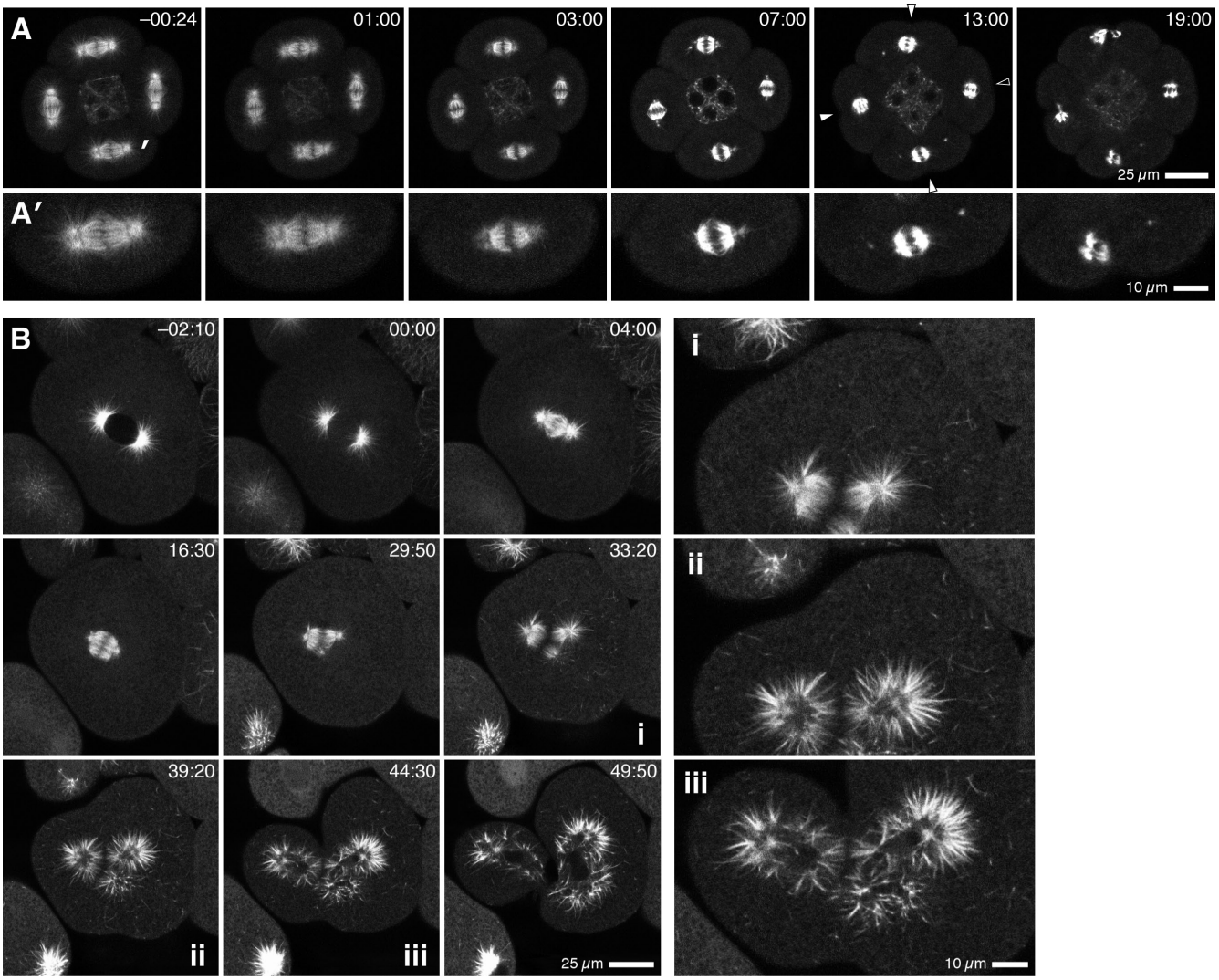

Figure S4. **Cleavage occurs even after extreme or prolonged loss of astral microtubules.** Single confocal sections; EMTB-3G. (A and A′) 16-cell purple urchin embryo treated with 40 μM TSA at time 00:00; A′ shows a 2× enlarged view of the southern cell (indicated by the white mark). All four cells entered anaphase, but extremely reduced spindle length with a very small midzone gap suggests minimal chromatid separation (compare with similar cases in Fig. 5). Virtually no astral microtubules survived, and some centrosomes separated from the spindle (bright dots in the 13:00 frame). Nonetheless, all cells initiated furrows at the right place (arrowheads, 13:00), only one of which regressed (open arrowheads), whereas the other three of the four completed (19:00). (B) One of eight cells in a slightly compressed sand dollar embryo treated with 20 μM TSA at time 00:00, before nuclear envelope breakdown. After an exceptionally long metaphase (>20 min) with no long astral microtubules, and during which one half of the spindle bifurcated, this cell entered anaphase ~26 min after TSA addition. Some astral microtubules regrew in anaphase, but none approach within 10 μm of the cortex. 2× enlarged views in i–iii show the half of the cell on which the furrow appears first. Furrowing began, as in normal cells, around the time that chromosomes began to decondense, forming vesicles near centrosomes (39:20). Despite obvious derangement of the mitotic apparatus and a long delay, the furrow successfully partitioned daughter nuclei. Video 4 includes A and B. Time is shown in minutes:seconds.

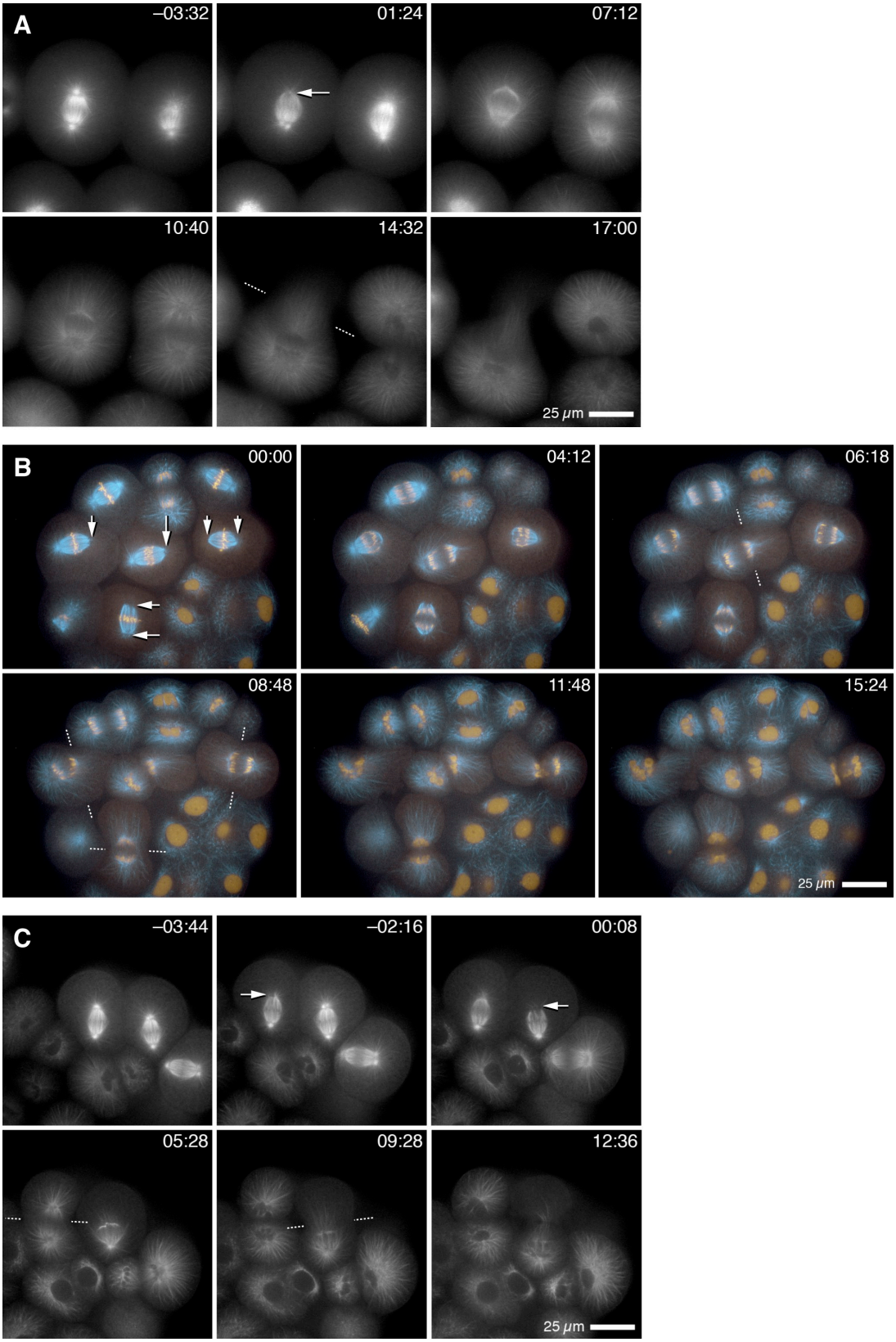

Figure S5. **Additional cases of centrosome ablation.** Single-plane recordings of sand dollar embryos; times are given in minutes:seconds after the end of irradiation. Arrows, ablated centrosome; dotted lines, cleavage plane. (A) An extreme single-pole ablation: virtually no astral microtubules remain in the ablated pole, and the ablated spindle half shrivels. Furrowing occurs beyond the ablated end of the mitotic spindle. See Video 7. (B) Mix of normal, two singly ablated, and two doubly ablated cells in an embryo (cyan, EMTB-3G; yellow, mC-H2B) showing chromosome segregation despite pole ablation. Both singly ablated cells exhibit shifts of the furrow toward the ablated pole, although in one cell, a correction makes the furrow partition chromosomes. Both doubly ablated cells make broad furrows; those furrows cross the spindle midzone, but in one cell, the chromosomes are not separated enough to be accurately partitioned (see Video 8). (C) Two single-pole ablations, contrasting a cell with substantial astral regrowth with a cell in which ablation is more complete. All three mitotic cells shown here were preparing to divide unequally, probably representing delayed micromere formation in this 32-cell embryo. The left cell redevelops the ablated aster, and cleavage proceeds with only a subtle shift of furrow relative to midzone. The middle cell retains no aster around the ablated pole, and the furrow forms and passes beyond the remains of the mitotic apparatus.

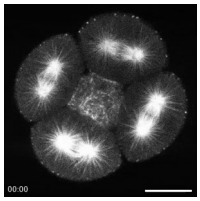

Video 1. **Ensconsin-3xGFP in normal urchin embryos.** The three sequences correspond to Fig. 1 (A–C). All are time-lapse sequences of single confocal sections (Radiance 2000; Bio-Rad Laboratories). First segment, purple urchin 16-cell embryo; second segment, sand dollar 28-cell embryo; third segment, sand dollar eight-cell embryo. Real times are indicated, and the video is encoded at 15 frames/s. Bars, 25 μm.

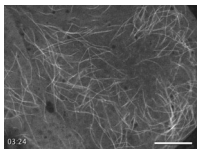

Video 2. **Ensconsin-3xGFP in a normal *X. laevis* blastomere.** The video corresponds to Fig. S1 D: time-lapse sequence of single superficial confocal section (MRC1024; Bio-Rad Laboratories). Real times are indicated, and the video is encoded at 15 frames/s. Bar, 25 μm

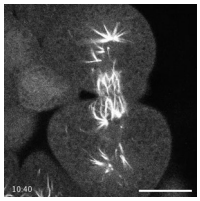

Video 3. **Urchin embryos expressing ensconsin-3xGFP treated with nocodazole at anaphase.** Time-lapse sequences of single confocal sections (Radiance 2000; Bio-Rad Laboratories). First segment (Fig. 3 A), eight-cell purple urchin embryo treated with 20 μM nocodazole at time 00:00. Second segment (no corresponding figure), eight-cell purple urchin embryo treated with 20 μM nocodazole at time 00:00. Third segment (Fig. 3 B), 16-cell purple urchin embryo treated with 10 μM nocodazole at time 00:00. Fourth segment (Fig. 3 C), 16-cell sand dollar embryo treated with 10 μM nocodazole at time 00:00. Fifth segment (Fig. 3 C), enlarged view of eastern cell from previous segment. Real times are indicated, and the video is encoded at 15 frames/s. Bars, 25 μm.

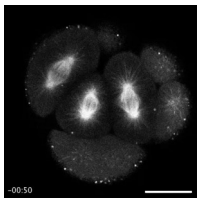

Video 4. **Urchin embryos expressing ensconsin-3xGFP treated with TSA.** Time-lapse sequences of single confocal sections (Radiance 2000; Bio-Rad Laboratories). First segment (Fig. 4 A), 16-cell purple urchin embryo treated with 20 μM TSA at time 00:00. Second segment (Fig. 4 C), one cell within a 16-cell sand dollar embryo treated with 25 μM TSA 10 min before time 00:00. Third segment (Fig. S4 A), 16-cell purple urchin embryo treated with 40 μM TSA at time 00:00. Fourth segment (Fig. S4 B), one cell in an eight-cell sand dollar embryo treated with 20 μM TSA at time 00:00. Real times are indicated, and the video is encoded at 15 frames/s. Bars, 25 μm

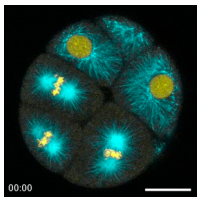

Video 5. **Urchin embryos coexpressing ensconsin-3xGFP and mC-H2B, normal versus TSA treated.** Time-lapse sequences of single confocal sections (Radiance 2000; Bio-Rad Laboratories) with EMTB-3G (microtubules) in shown cyan and mC-H2B (chromatin) in yellow. First segment (Fig. S3 A), untreated 16-cell purple urchin embryo. Second segment: (Fig. S3 B), 16-cell purple urchin embryo treated with 15 μM TSA at time 00:00. Real times are indicated, and the video is encoded at 15 frames/s. Bars, 25 μm.

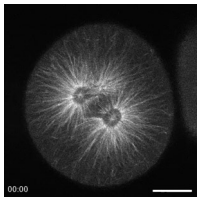

Video 6. **Anucleate sand dollar cytoplasts expressing ensconsin-3xGFP.** Time-lapse sequences of single confocal sections (Radiance 2000; Bio-Rad Laboratories). Three segments correspond to Fig. 7 (A–C). Real times are indicated, and the video is encoded at 15 frames/s. Bars, 25 μm.

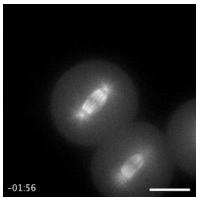

Video 7. **Ablation of single centrosomes in sand dollar blastomeres expressing ensconsin-3xGFP.** Time-lapse sequences of single confocal sections (CARV; BD). The first segment corresponds to Fig. 8 A, the second segment is a similar case for which there is no corresponding figure, and the third segment corresponds to Fig. S5A. Real times are indicated, and the video is encoded at 15 frames/s. Bars, 25 µm.

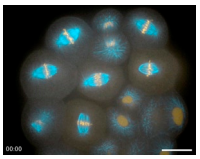

Video 8. **Single and double centrosome ablations in a sand dollar embryo coexpressing ensconsin-3xGFP (cyan) and mC-H2B (yellow).** Time-lapse sequence of single confocal sections (CARV; BD). Video corresponds to Fig. S5 B. Real times are indicated, and the video is encoded at 15 frames/s. Bar, 25 µm.

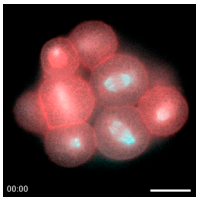

Video 9. **Centrosome ablation in sand dollar blastomeres coexpressing GFP-rGBD (red) and ensconsin-3xGFP (cyan).** Time-lapse sequences of single confocal sections (CARV; BD). First segment (Fig. 8 B): two single ablations surrounded by normal cells. Second segment (Fig. 8 D): one normal, one singly ablated, and one doubly ablated cell. Third segment (Fig. 8 C): doubly ablated cell. Real times are indicated, and the video is encoded at 15 frames/s. Bars, 25 µm.